High-pressure granulite facies metamorphism (~1.8 GPa) revealed in silica-undersaturated garnet-spinel-corundum gneiss, Central Maine Terrane, Connecticut, U.S.A.

DUNCAN S. KELLER^{1,*} AND JAY J. AGUE¹

Department of Geology and Geophysics, Yale University, PO Box 208109, New Haven, Connecticut 06520-8109, U.S.A.

ABSTRACT

We quantify the metamorphic pressure-temperature (P-T) conditions for a newly discovered silicaundersaturated high-pressure granulite (HPG) from the Central Maine Terrane (CMT) in northeastern Connecticut, U.S.A. The rocks lie within the Acadian-Neoacadian orogenic belt (Devonian) and form part of the Brimfield Schist. The Brimfield and the adjacent Bigelow Brook Formation contain silica-saturated rocks that have previously been shown to have undergone ~1000 °C metamorphism. The pressure was less well constrained at ≥ ~1 GPa. Silica-undersaturated rocks hold underutilized potential for pinpointing peak metamorphic conditions, particularly pressure, because of their resilience to melting and the variety of refractory minerals they contain. The typical silica-undersaturated mineral assemblage is garnet + spinel + corundum + plagioclase + K-feldspar + biotite + ilmenite. Leucosomes are syenites consisting of two feldspars ± biotite. Plagioclase is commonly antiperthitic, particularly in feldspathic domains surrounding peritectic garnet; such garnet crystals reach ~10 cm in diameter. Alkali feldspars are perthitic. The rocks contain remarkable ellipsoidal spinels as much as 5.5 cm long comprising discrete crystallographic domains hosting crystallographically oriented lamellae of a Fe-Ti phase, most likely ilmenite. Corundum is usually colorless, but can also be found as sapphire in shades of pink, purple, and blue, particularly in antiperthite-rich domains surrounding large garnets. Some sapphires are concentrically color zoned. We carried out a P-T estimation using ternary feldspar reintegration thermometry of metamorphic antiperthites together with pseudosection modeling. Samples texturally and chemically record near-eclogite facies equilibration at minimum conditions of ~1040 °C and ~1.8 GPa, establishing the CMT in northeastern CT as the first known HPG locality in the U.S. These results are consistent with high P_2O_5 levels found in garnet (0.18 wt%), Ti-in-biotite thermometry, regional sillimanite pseudomorphs after kyanite, and preliminary experimental work on melt inclusions in garnet (Ferrero et al. 2017). The leucosomes provide strong evidence that partial melting of silica-undersaturated rocks at HPG conditions can produce syenitic magmata. Strongly melt-depleted silica-undersaturated rocks may also be protoliths for garnet + spinel + corundum xenoliths reported from kimberlites. The presence of HPG gneisses demonstrates that the large-scale thrusts of the CMT sample the deepest roots of the orogenic belt (60-70 km), and perhaps even deeper subduction zone lithologies as well.

Keywords: High-pressure granulite, silica-undersaturated, corundum, spinel, garnet, syenite

Introduction

High-pressure granulites (HPG) form at or below the base of orogenically thickened crust at pressures $(P) \ge 1.5$ GPa and temperatures (T) \geq 850 °C in the stability field of kyanite, commonly at eclogite facies conditions (O'Brien and Rötzler 2003). They provide textural, chemical, and mineralogical records of lower crustal processes and environments, and they are particularly valuable tools for evaluating models of how mountain belts form, the depths to which continental material can be underthrust and potentially subducted, and how rocks are exhumed from deep crustal levels. Although HPGs are reported from many orogenic belts worldwide (see O'Brien and Rötzler 2003; Kotková 2007, and references therein) none have been identified in the U.S. Paleoproterozoic HPGs are present in the Snowbird tectonic zone of Canada (Snoeyenbos et al. 1995; Baldwin et al. 2003), and Neoproterozoic HPGs (and eclogites) are present in the Grenville orogen of eastern Canada (Indares 1993, 1995, 1997; Indares et al. 1998; Indares and Dunning 2001). The lack of high-pressure granulites in the northeastern U.S.A. is particularly conspicuous, as granulites are a significant component of the Acadian-Neoacadian orogen in the Central Maine Terrane (Peper and Pease 1975; Fahey and Pease 1977; Chamberlain and England 1985; Schumacher et al. 1989; Robinson et al. 1998).

Recent experimental evidence suggests, however, that silicic ultrahigh-temperature granulites of the Brimfield Schist and Upper Member of the Bigelow Brook Formation in northeastern Connecticut, part of the Central Maine Terrane (Ague et al. 2013; Axler and Ague 2015a) underwent early HPG metamorphism (Ferrero et al. 2017). Re-homogenization of quartz-bearing melt inclusions indicates that for a T of 1050 °C (Axler and Ague 2015a) melt entrapment occurred at $P \ge 1.7$ GPa (Ferrero et al. 2017). These conditions exceed the canonical pressure limit of UHT metamorphism (Harley 1998; Brown 2006; Kelsey 2008) and easily reach the high-pressure granulite facies. This result is preliminary, but nonetheless offers a tantalizing glimpse of higher-pressure metamorphism than has been previously reported in the orogen.

Independent corroboration of this *P* estimate is necessary to establish the nature and extent of HPG metamorphism within the

^{*} E-mail: duncan.keller@yale.edu

orogen. However, the matrix assemblage of the quartz-bearing granulites does not provide a robust pressure constraint other than the rutile/ilmenite transition, yielding minimum $P \sim 1$ GPa (Ague et al. 2013). Distinguishing ultrahigh-temperature (UHT) rocks from HPGs represents a particular challenge because unless HPG indicator minerals like kyanite form and are preserved, many intermediate and felsic bulk compositions crystallize quartzofeldspathic garnet-bearing assemblages that are not strongly diagnostic of pressure at ~1000 °C and 1–2 GPa. In fact, the type locality granulites from the Granulitgebirge of Saxony, Germany, were only recently recognized as HPGs, based on petrographic observations coupled with modern geothermobarometric and modeling techniques (e.g., Rötzler 1992; Rötzler and Romer 2001; O'Brien 2006; Müller et al. 2015). Silica-undersaturated rocks, however, have the potential to provide independent P-T constraints at UHT and HPG conditions (e.g., Kelsey et al. 2005; Kelsey 2008; Dorfler et al. 2015; Guevara and Caddick 2016).

In particular, silica-undersaturated rocks that contain coexisting garnet, spinel, and corundum hold significant promise for revealing P-T histories. Such rocks are not commonly described in the literature, but are nonetheless reported from several field areas worldwide including in India (Harris 1981; Sengupta et al. 1999; Shimpo et al. 2006), Sri Lanka (Osanai et al. 2006; Dharmapriya et al. 2015), Algeria (Ouzegane et al. 2003), South Africa (Schreyer et al. 1984), Antarctica (Asami et al. 1989, 1990), the U.S. (Cortland complex; e.g., Dorfler et al. 2014, 2015), and Canada (Snoeyenbos et al. 1995). Roof pendants in the Vinalhaven pluton (Maine, U.S.A.) contain garnet, spinel, and corundum, but these minerals do not form a distinct assemblage; garnet is only present in leucosomes with quartz (Porter et al. 1999). Retrogressed eclogite from the Trans-Hudson orogen contains garnet with spinel ± corundum (+ plagioclase) symplectites after kyanite (Weller and St-Onge 2017). Kimberlite pipes have yielded bi- to tri-mineralic garnet ± spinel ± corundum xenoliths that can contain centimeter-scale colored corundum and are generally interpreted as mantle cumulates or extremely melt-depleted metapelites sourced from slabs (Nixon et al. 1978; Padovani and Tracy 1981; Exley et al. 1983; Mazzone and Haggerty 1989).

In this paper, we describe a newly discovered silica-under-saturated lithology (Table 1) from the Central Maine Terrane, Connecticut (CT), which contains porphyroblastic garnet, spinel, and corundum. The rocks are part of the same litho-tectonic rock sequence in which Ague et al. (2013) and Axler and Ague (2015a) determined extreme metamorphic $T\sim1000\,^{\circ}$ C. We evaluate equilibration P-T conditions using ternary feldspar reintegration thermometry and pseudosection modeling in conjunction with textural observations. The results demonstrate that the rocks reached HPG conditions, the first in situ HPG example we are aware of in the U.S. If the silica-saturated rocks studied by Axler and Ague (2015a) and Ferrero et al. (2017) are also HPG, then multiple HPG localities exist in the Central Maine Terrane. We then discuss the tectonic implications of HPG rocks within the Central Maine Terrane and the potential of these rock types to elucidate lower crustal processes.

GEOLOGIC SETTING

The Brimfield Schist hosts the rocks of this study and is one of several rock units cut and/or bounded by west-northwestdipping thrust faults within the southern Central Maine Terrane

TABLE 1. Bulk compositions of samples used for pseudosection modeling

	Type I	—— Ту	/pe II ——
	150A	268A	269A
SiO ₂ (wt%)	38.63	40.80	44.10
TiO ₂	2.38	2.18	1.94
Al_2O_3	27.69	24.90	23.00
FeO(tot)	18.74	17.38	16.39
Fe_2O_3	0.21	0.19	0.18
FeO	18.53	17.19	16.21
MgO	2.94	4.01	3.60
MnO	0.19	0.07	0.07
CaO	0.74	0.32	0.88
Na₂O	0.65	0.66	1.16
K ₂ O	6.19	7.97	7.39
P_2O_5	0.35	0.14	0.13
LOI	1.79	2.15	2.12
Total	99.94	100.44	100.65
mol Fe ³⁺ /Fe(tot)	0.01	0.01	0.01
Density @ 1040 °C, 1.8 GPa (g/cm ³)	3.09	2.98	2.95
Density (-50% melt)	3.25	3.09	3.05
Density (-100% melt)	3.52	3.26	3.22

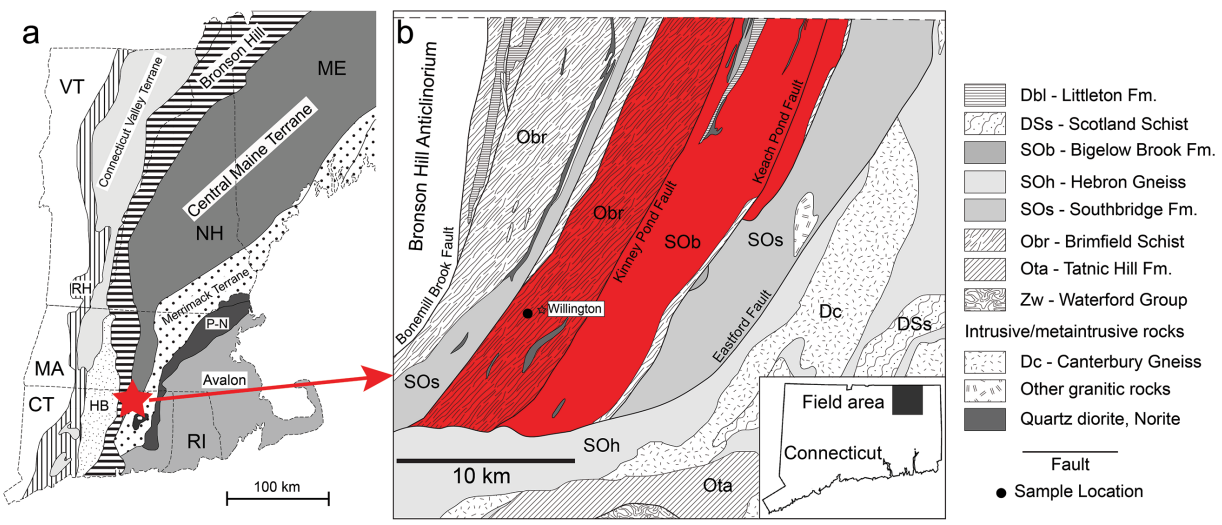
Notes: Compositions were obtained by X-ray fluorescence (XRF). CaO adjusted assuming all P_2O_5 is hosted in apatite. LOI denotes loss on ignition, and is recalculated from raw values to account for Fe_2O_3 created during XRF combustion assuming $Fe^{3\nu}/Fe(tot)$ ratio of 0.01 (see Analytical Methods). Densities calculated using Theriak-Domino.

(CMT; also known as, for example, the Merrimack Synclinorium, e.g., Rodgers 1981, and the Central Maine belt, e.g., Robinson et al. 1998). Together with the other rock units in this area it reached or exceeded granulite facies metamorphic conditions (Tracy et al. 1976; Robinson 1978; Rodgers 1981; Ague et al. 2013) (Fig. 1). The Brimfield Schist and its internal shear zones contain a wide variety of lithologies including aluminous and quartzofeldspathic gneisses, granitoids, amphibolites, ultramafic blocks, rare metacarbonate rocks, and the silica-undersaturated rocks described herein (Ague et al. 2013).

Silica-saturated metapelitic gneisses of the Brimfield Schist and the adjacent Bigelow Brook Formation record a UHT signature (Ague et al. 2013; Axler and Ague 2015a). These rocks locally preserve a matrix assemblage with spinel and cordierite from this phase of metamorphism, stable at ~0.6 GPa. As noted above, however, recent melt-inclusion re-homogenization experiments show that a HPG stage (~1050 °C; 1.7–2.0 GPa) likely pre-dated UHT metamorphism in the Bigelow Brook Formation (Ferrero et al. 2017). Sillimanite pseudomorphs after kyanite are preserved in metapelitic gneisses of the Brimfield Schist and Bigelow Brook Formation (Peper and Pease 1975; Fahey and Pease 1977; Axler and Ague 2015a). This is consistent with overprinting of kyanite-bearing HPG assemblages by later, lower-pressure, UHT metamorphism.

Additional metamorphic overprints have affected the region. A 700–800 °C, 0.5–0.6 GPa granulite facies signature was recognized by Ague et al. (2013) as post-dating the UHT signature of quartz-bearing metapelitic gneisses from the Brimfield Schist. Following this, a kyanite zone overprint is evident from metasomatic kyanite-garnet-quartz-carbonate veins that cut across several lithologies within the Brimfield Schist, together with other regional occurrences of texturally late kyanite (Schumacher et al. 1989; Ague 1995; Thomson 2001).

Field relationships and geochronology document Acadian (~420–380 Ma) and Neoacadian (~360 Ma) metamorphism in the CMT (e.g., Rodgers 1981; Robinson and Tucker 1982;



Ague & Eckert (2012 AmMin): Ague et al. (2013 Geology); Axler & Ague (2015a JMG, 2015b AmMin)

FIGURE 1. Geologic map showing (**a**) Major geologic terranes of New England, U.S.A., following Axler [unpublished Ph.D. thesis; after Aleinikoff et al. (2007) as modified from Hibbard et al. (2006)]. (**b**) Sample location within thrust slices of the Central Maine Terrane. Formations colored in red are UHT (Ague et al. 2013; Axler and Ague 2015a; based on geologic maps of Rodgers 1981, 1985). HB = Hartford Basin, RH = Rowe-Hawley, P-N = Putnam-Nashoba. (Color online.)

Schumacher et al. 1989; Armstrong et al. 1992; Getty and Gromet 1992; Wintsch et al. 1992, 2009; Robinson et al. 1998; Thomson 2001; Massey et al. 2017). Both of these events are recognized in metamorphic zircon from the Brimfield Schist and Bigelow Brook Formation, with the Neoacadian signal being dominant (Axler and Ague 2015c; Axler, unpublished Ph.D. thesis). Rodgers (1981) suggested that the southern CMT originated in an accretionary prism formed during westward subduction before the Acadian collision, but this interpretation is not universally accepted (Robinson and Tucker 1982).

Elsewhere in the eastern U.S., silica-undersaturated metapelitic or metagranitic rocks are found only in a handful of localities, including the Ordovician Cortlandt Complex (e.g., Rogers 1911; Barker 1964; Dorfler et al. 2014; Dorfler et al. 2015), the Silurian Cadillac Mountain granite (Nichols and Wiebe 1998), and the Siluro-Devonian Calderwood Neck Pendant in the Vinalhaven Pluton (Porter et al. 1999).

ANALYTICAL METHODS

Quantitative mineral chemistry and backscattered electron (BSE) images were collected with a JEOL JXA-8530F field emission gun electron probe microanalyzer (EPMA) in the Yale University Department of Geology and Geophysics. Wavelength-dispersive spectroscopy (WDS) was used for all mineral chemistry and elemental maps; quantitative analyses employed natural and synthetic standards and off-peak background corrections. Operating conditions were 15 kV accelerating voltage and 10.8 mm working distance with a focused beam. Beam current was 10 nA for biotite and feldspars, 20 nA for oxides, and 50 nA for garnet. Element mapping used a beam current of 20 nA and a dwell time of 100 ms for corundum, 200 nA and 100 ms for lower-resolution garnet maps and the spinel map, and 300 nA and 200 ms for the high-resolution garnet phosphorus map. Spinel host and oxide lamellae were reintegrated using an evenly spaced grid of 24 unfocused (25 μ m) beam spots.

Ternary feldspar compositions for leucosome and matrix antiperthites were reconstructed following Ague et al. (2013). Compositions of host and lamellae were measured via EPMA, and (BSE) images of each grain were captured. Proportions of host and lamellae were determined by analyzing the BSE images in ImageJ

(U.S.A. National Institutes of Health, https://imagej.nih.gov/ij, accessed Aug 15, 2017). Precursor compositions were then calculated from EPMA data using host and lamellae proportions, assuming a representative cross section. In the rare case that an antiperthite grain rim lacked lamellae, the rim was excluded from the calculation. Perthites were reintegrated using two techniques. The conservative reintegration counted only preserved lamellae in perthite hosts, and used evenly spaced grids of unfocused (25 um) beam spots (Table 2). Image processing was not used for this group because they have irregularly distributed lamellae on several scales, from micrometers to sub-micrometers wide, as well as low BSE contrast between K-feldspar host and lamellae that complicates image processing. A test case for two-feldspar thermometry counted grain boundary plagioclase as well as lamellae for a well-preserved example (Table 3), and used spot analyses of host and lamellae combined with image analysis. Ternary feldspar temperature estimates were calculated using Theriak/Domino ver. 3.1 (De Capitani and Petrakakis 2010) with the feldspar activity models of Benisek et al. (2004, 2010). Two-feldspar thermometry for antiperthite-perthite+reintegrated grain boundary plagioclase used the method of Benisek et al. (2010), after Kroll et al. (1993).

Bulk-rock chemistry (Table 1) was measured via X-ray fluorescence (XRF) of representative samples (150A/268A/269A) by SGS (see Ague 2011 and references therein for analytical details). Measured CaO was reduced assuming all P_2O_3 is hosted in apatite and LOI (taken to be H_2O) was re-calculated from the raw data based on a fixed Fe^{3+}/Fe (total) molar ratio. This ratio was deduced for each sample by comparing measured ilmenite compositions to those predicted by phase equilibrium calculations for a given Fe^{3+}/Fe (total) molar ratio (see Results section). Assuming ilmenite equilibration between the peak metamorphic conditions estimated herein and later lower granulite facies conditions along the P-T path of the Brimfield Schist (Ague et al. 2013) gives a Fe^{3+}/Fe (total) molar ratio of 1%. The phase relations are relatively insensitive to the Fe^{3+}/Fe^{2+} (total) ratio; values up to \sim 10% have no significant effect on the P-T estimates.

Pseudosection modeling used Theriak/Domino ver. 4.02 (De Capitani and Petrakakis 2010) and the thermodynamic data file of D.K. Tinkham (ver. 02, http://dtinkham.net/peq.html#theriak-domino-files-holland-powell-2011-database, accessed August 24, 2015) that contains the internally consistent tc-ds62 thermodynamic database of Holland and Powell (2011; referred to herein as HP11) and compatible activity models. The following activity models were used: melt (White et al. 2014a); ternary feldspar (Holland and Powell 2003); garnet (White et al. 2014a, 2014b); white mica (White et al. 2014a); biotite (White et al. 2014a, 2014b); croflierite (White et al. 2014a, 2014b); sapphirine (Wheller and Powell 2014); cordierite (White et al. 2014a, 2014b); spinel (White et al. 2002); ilmenite (White et al. 2014b). The clinopyroxene model of Holland and Powell (1996) was used

TABLE 2.	Reintegrated perthite co	mpositions measured	d by beam grids			
Sample	294A-1 ^a n = 25	294A-1 ^a n = 25	294A-1 n = 25	294A-3 n = 25	312A-1 n = 25	312A-1 n = 25
SiO ₂	64.30(0.35)	64.29(0.27)	64.34(0.35)	64.41(0.17)	64.10(0.35)	64.70(0.16)
P_2O_5	0.29(0.03)	0.34(0.04)	0.34(0.22)	0.25(0.03)	0.19(0.02)	0.20(0.03)
AI_2O_3	19.48(0.44)	19.39(0.31)	19.30(0.23)	19.19(0.10)	19.35(0.34)	19.61(0.17)
FeO	0.02(0.02)	0.02(0.03)	0.03(0.03)	0.04(0.03)	0.03(0.04)	0.09(0.03)
MgO	b.d.	b.d.	0.01(0.01)	b.d.	0.01(0.02)	0.02(0.01)
MnO	0.01(0.02)	0.01(0.02)	0.01(0.01)	0.01(0.02)	0.01(0.02)	0.01(0.02)
CaO	0.40(0.43)	0.28(0.30)	0.40(0.30)	0.22(0.04)	0.48(0.25)	0.45(0.12)
BaO	0.14(0.03)	0.15(0.03)	0.14(0.04)	0.19(0.03)	0.40(0.05)	0.38(0.04)
Na₂O	2.13(0.48)	1.96(0.32)	2.36(0.35)	1.76(0.06)	3.01(0.60)	3.08(0.35)
K₂O	13.43(1.03)	13.76(0.69)	13.17(0.59)	14.01(0.13)	12.02(1.01)	11.91(0.56)
Total	100.20(0.25)	100.20(0.23)	100.10(0.27)	100.09(0.22)	99.61(0.43)	100.45(0.19)
			Structural formulas (8	3 O)		
Si	2.943	2.945	2.946	2.957	2.945	2.944
Р	0.011	0.013	0.013	0.010	0.007	0.008
Al	1.051	1.047	1.041	1.038	1.048	1.052
Fe	0.001	0.001	0.001	0.002	0.001	0.003
Mg					0.001	0.001
Mn					0.001	
Ca	0.020	0.014	0.020	0.011	0.024	0.022
Ba	0.003	0.003	0.003	0.003	0.007	0.007
Na	0.189	0.174	0.210	0.157	0.268	0.272
K	0.784	0.804	0.769	0.820	0.705	0.691

TABLE 2. Reintegrated perthite compositions measured by beam grids

Notes: b.d. = below detection. 20 standard deviations given in parentheses. All Fe as FeO. analyses come from two different portions of the same grain.

for simplicity and, thus, clinopyroxene phase relations should be regarded with caution. This has no impact on our conclusions as the *P-T* conditions recorded by the rocks are well outside the stability field of clinopyroxene. Importantly, HP11 is applicable to HPG conditions (White et al. 2014a).

RESULTS

Rock description and field relations

The dominant matrix mineral assemblage is garnet + spinel + corundum + K-feldspar + biotite + ilmenite, with leucosomes of two feldspars ± biotite in veins and/or surrounding garnet. The rock crops out as a single, uneven horizon several meters thick bounded by more siliceous, quartz-bearing gneisses. A fault marks the lower contact with the silicic gneiss. The upper contact, with a dark gray gneiss, is obscured by meter-scale leucosomes. Sheared leucosomes document thrust motion with a transport direction toward the modern E-SE (Fig. 2a).

The rocks vary from coarsely foliated to massive (Figs. 3a and 3e). Two textural styles are recognized: Type I is a "salt-and-pepper" variety where alkali feldspar is evenly distributed throughout the matrix (Fig. 3e), and Type II has uneven alkali feldspar distribution with coarse and interconnected leucosomes often defining a foliation (Fig. 3a). Leucosomes in Type I samples commonly have disaggregated edges. Both types contain the same mineral assemblage, although Type II contains the coarsest garnet, spinel, and corundum. In Type II samples, fine-grained bands several millimeters thick with numerous idiomorphic garnets and extremely fine-grained biotite suggest localized shearing; in some of these regions, garnet porphyroblasts show trails and crusts of idiomorphic garnets in thin section (Fig. 4a). Most Type II samples contain trace pyrrhotite, chalcopyrite, and other sulfides in the matrix and as inclusions in corundum.

The chemical characteristics of the rocks likely reflect those of the protolith (e.g., some type of aluminous sediment or volcaniclastic deposit) modified by melt loss leading to silica undersaturation (e.g., Clifford et al. 1975; Lal et al. 1978; Grant 1985a, 1985b) prior to the HPG stage. Protolith identification must await further geochemical study.

Mineral descriptions and chemistry

Garnet. Garnet is found mainly as isolated crystals and has sharp contacts with spinel and/or corundum with no intervening coronas or reaction zones (Figs. 3d and 4b). Megacrystic (up to ~10 cm) garnets occur within a sheared portion of the unit (Fig. 2b). In some samples, small (~100–300 μm) subhedral to euhedral garnets are present in addition to larger porphyroblasts (Fig. 4a). Garnet interiors commonly include grains of embayed spinel (Figs. 4a and 5a), former ternary feldspar (now with exsolution features, Fig. 6), apatite, biotite, ilmenite, and, very rarely, sillimanite. Some garnet rims contain sillimanite, corundum, biotite, and spinel inclusions. Some garnets are partially altered to chlorite along cracks and rims but are otherwise fresh. Garnets rimmed by leucosomes are inferred to be peritectic; these include the megacrystic variety in Figure 2b. Some peritectic garnet rims include antiperthites (Fig. 7a).

Representative garnet compositions are given in Supplemental¹ Table S1. Garnet is almandine rich and often shows Mn depletion in rims (Supplemental¹ Table S1) as well as Mg depletion near contacts with biotite and along infilled cracks (Fig. 6c). Overall, garnets preserve little core-to-rim variation in Fe, Mg, and Ca. Where zonation of these elements is preserved, it is smooth, almost certainly reflecting diffusional relaxation (Figs. 6b–6d).

Notably, some garnets have distinctly elevated phosphorus contents. In particular, the core of garnet in sample 294A-1 contains 0.18 wt% P_2O_3 (Supplemental¹ Table S1). Moreover, this garnet preserves a detailed textural record of modifications to zonation. The element map reveals that phosphorus is complexly and irregularly zoned in the garnet core, but a more regular core-to-rim zonation pattern is preserved in the bottom-left quadrant (Fig. 6b). The highest-phosphorus area has a sharp and irregular contact with the low-phosphorus area, showing lobate and irregular zoning comparable to that produced by interface-coupled dissolution-reprecipitation (ICDR) in garnets from UHP and HP granulites (Ague and Axler 2016). The ICDR process requires the interaction of fluids (defined broadly to also

TABLE 3. Reintegrated ternary feldspar compositions plotted in Figure 9

riguic	,						
		Per	thite				
Sample	294A-1	294A-1	294A-1	294A-3	312A-1	312A-1	278A-1
Plotting code	Α	В	C	D	E	F	Т
Kfs	79.0	81.0	77.0	83.1	70.2	70.7	77.3
Ab	19.0	17.6	21.0	15.9	27.6	26.9	16.5
An	2.0	1.4	2.0	1.1	2.2	2.4	6.2
T(°C) @ 1.5 GPa [B10]	893	848	885	822	874	886	1118
T(°C) @ 1.5 GPa [B04]	780	738	792	707	840	843	914
		Antip	erthite				
Sample	150A-2	271A-1	278A-1	278A-1	278A-1	281A-1	
Plotting code	1	2	3	4	5	6	
Kfs	16.1	22.8	18.9	19.3	23.2	18.3	
Ab	52.7	42.7	46.9	47.0	44.9	48.6	
An	31.2	34.5	34.2	33.7	31.9	33.1	
T(°C) @ 1.5 GPa [B10]	979	1114	1055	1054	1084	1034	
T(°C) @ 1.5 GPa [B04]	985	1050	1019	1022	1047	1012	
Two-feldspar T			1059	1058	1073/		
					1001		

Notes: Abbreviations of feldspar models are B04 = Benisek et al. (2004) and B10 = Benisek et al. (2010). Perthite compositions are averages of grid analyses (Table 2) except 278A-1 plotting code T, which is based on spot analyses of host and grain boundary plagioclase (Table 4) reintegrated following the procedure used for antiperthite. K-feldspar (Kfs), albite (Ab), and anorthite (An) are given in mol%. Two-feldspar T estimates all use the same Kfs composition (278A-1 plotting code T). Plotting codes refer to Figure 9.

include melts) with minerals (e.g., Putnis and Austrheim 2010; Putnis and John 2010; Harlov et al. 2011). Thus, the isolated zones of phosphorus-rich garnet are likely relics of incomplete reactions with infiltrating fluid. A faint core-to-rim zoning of phosphorus is preserved in the bottom-right quadrant of the high-phosphorus region (Fig. 6b), suggesting that this is the original growth zoning and the low-phosphorus zones have been leached.

The core of the high-phosphorus garnet in sample 294A-1 contains oriented lamellae of rutile, ilmenite, and apatite. The lamellae are restricted to the phosphorus-rich portion of the garnet and are absent from immediately adjacent areas with lower phosphorus contents. They are oriented in four major directions and several subsidiary directions; the four major directions correspond to the <111> axes of the garnet host (e.g., Griffin et al. 1971; Axler and Ague 2015a). Some lamellae are composites of two minerals. Pairs of ilmenite with either apatite or rutile are present and show a range of morphologies (Fig. 4d).

Oriented rutile and ilmenite lamellae have been previously documented in garnet cores from the silica-saturated rocks in both the Brimfield Schist and the Bigelow Brook Formation (Ague and Eckert 2012; Ague et al. 2013; Axler and Ague 2015a). Depletion halos of Ti around these lamellae confirm an exsolution (precipitation) origin (Ague and Eckert 2012). For the silica-undersaturated lithology of this study, the restriction of lamellae to portions of garnet apparently unmodified by ICDR, their consistent lamellar habits, and their orientation along garnet zone axes, lead us to the interpretation that the inclusions exsolved from a precursor garnet richer in Ti and phosphorus; verification of this must await future crystallographic study.

Spinel. Spinel is found as black-green ragged, net-like matrix grains (\sim 500 μ m to 3 mm) and remarkable elongated, polycrystalline masses that reach nearly 6 cm in length (Figs. 3a and 3c) with long axes aligned roughly parallel to foliation. The largest grains contain thin (\leq 1 μ m) platelets of Fe-Ti oxide that are oriented in four directions and can have broadly trigonal





FIGURE 2. Field exposures of the silica-undersaturated rocks. Grt = garnet. (a) Sheared leucosome; arrows indicate thrust sense of shear. (b) Garnet megacrysts surrounded by leucosome. (Color online.)

cross sections. Oriented lamellae are largely absent in the rims of spinel masses and were not observed in spinel crystals less than ~1 mm wide. Within the large spinel masses, crystallographic domains on the order of several millimeters are distinguishable in hand sample by their different reflections of light and in thin section by changes in orientation of oriented oxide platelets (Fig. 5c). Larger spinels typically host inclusion pockets ~50 to ~500 µm across containing ternary feldspar with exsolution features, homogeneous feldspar, corundum, and biotite. Isolated feldspar inclusions are widespread.

Analyzed spinel is hercynite rich and usually Zn poor (\leq 0.5 wt%; Supplemental¹ Table S2). Spinel is notably Mg poor relative to many garnet-spinel-corundum-bearing rocks (e.g., Padovani and Tracy 1981; Sengupta et al. 1999; Dharmapriya et al. 2015), especially those containing sapphirine (e.g., Ouzegane et al. 2003). Matrix spinel generally has between 2 and 2.5 wt% MgO; spinels included in garnet have elevated MgO relative to those in the matrix (e.g., sample 268A-2; 4.5 wt%), even those in contact with garnet. Matrix spinel from sample 294A-1 has the highest Cr_2O_3 content (\sim 4.5 wt%), and particularly low MgO content (2.0 wt%).

The oriented oxide lamellae are too thin for individual EPMA analysis, but a reintegrated spinel composition was estimated

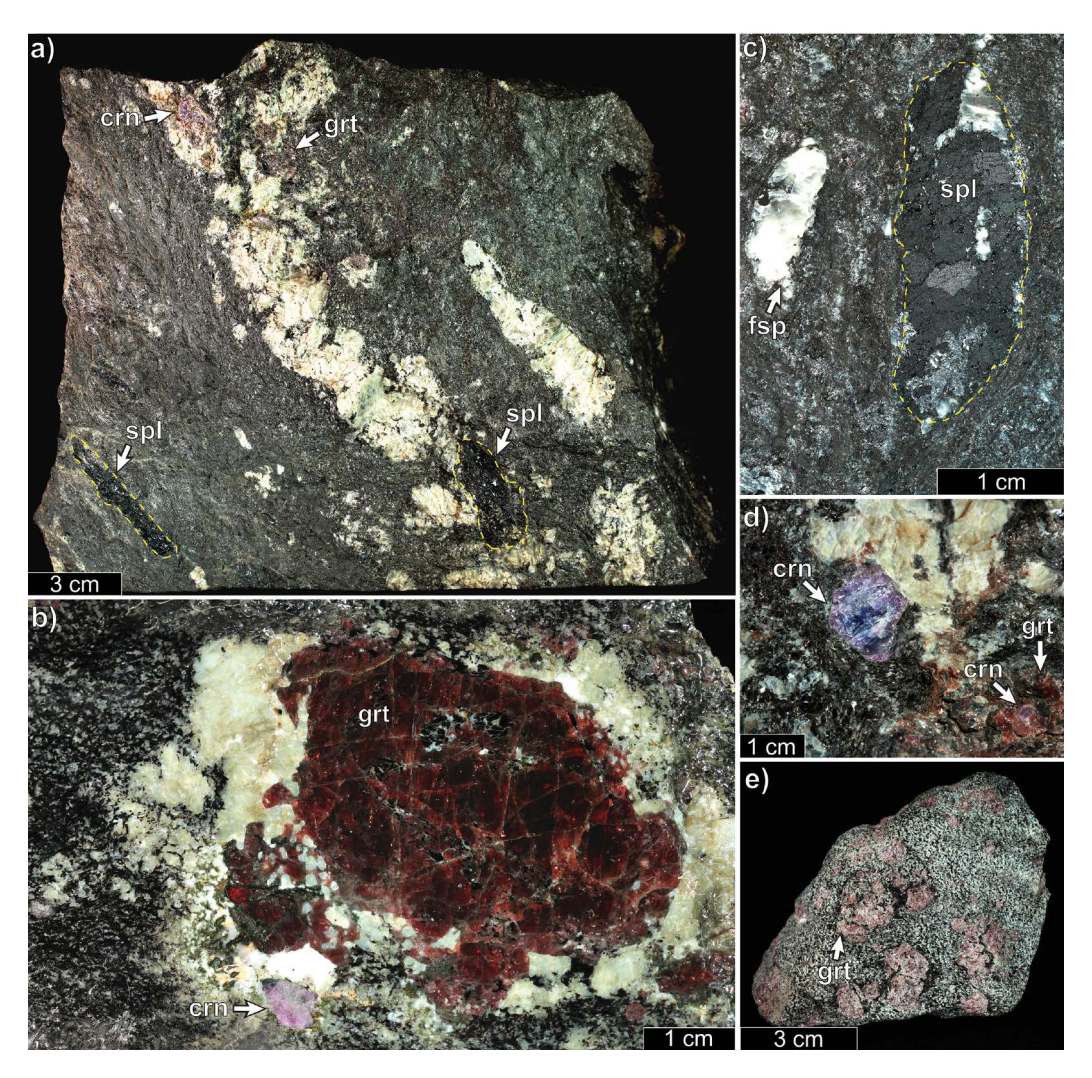


FIGURE 3. Silica-undersaturated rocks in hand sample. Grt = garnet, spl = spinel, crn = corundum, fsp = feldspar. (a) Type II sample showing coarse leucosomes and spinel defining foliation and pink-purple sapphires within leucosomes [296A]. (b) Peritectic garnet including antiperthite surrounded by antiperthite-bearing leucosome in contact with a pink sapphire; spinel and corundum are present in the matrix assemblage [295A]. (c) Spinel mass showing irregular crystallographic domains revealed by differential reflection of light [296A]. (d) Concentrically zoned sapphire in contact with leucosome and garnet that includes pink corundum [298A]. (e) Type I sample [150A]. (Color online.)

with regularly spaced spot analyses, yielding a bulk TiO_2 content of 0.1 wt% (Supplemental¹ Table S2). This analysis method may underestimate the proportions of elements preferentially sequestered in the lamellae based on lamellae orientations relative to the sectioned plane, although the beam spot (25 μ m diameter) was significantly larger than lamella width, and lamellae have a regular distribution within the host. We consider it likely that the lamellae exsolved to reduce spinel Ti content during retrogression.

Corundum. Corundum is present in two forms: as ≤1 cm subhedral to euhedral pink, purple, and blue crystals generally in contact with or within leucosomes in Type II samples (Fig. 3b and 3d), and colorless, jagged matrix grains often rimming spinel in both Type I and Type II samples (Figs. 4a and 5b). Both varieties have polysynthetic twinning in thin section and fluoresce red under long-wave ultraviolet light, with pink and purple crystals (or zones within crystals) showing stronger

fluorescence than blue or colorless ones. The largest sapphires have concentric color zoning in hand sample (Fig. 3d). Most corundum crystals are fresh, although some in leucosomes are coated with chlorite.

A Cr element map of a representative coarse pink corundum in contact with leucosome surrounding peritectic garnet (in a Type II sample) reveals euhedral concentric zoning suggesting growth in contact with a fluid, most likely silicate melt, which may have supplied the trace elements (Fe, Ti, Cr) responsible for coloration (Figs. 3b and 5e). The presence of large colored corundum crystals, which only occur in Type II samples, appears to be tied to the presence of coarse leucosome networks.

Colorless matrix corundum commonly includes biotite and spinel and has few impurities, with negligible SiO_2 , Fe_2O_3 , TiO_2 , and Cr_2O_3 contents (Supplemental¹ Table S3). Impurities are slightly higher in coarse, colored sapphire, but the mole fraction of corundum is >0.99 for all investigated crystals.

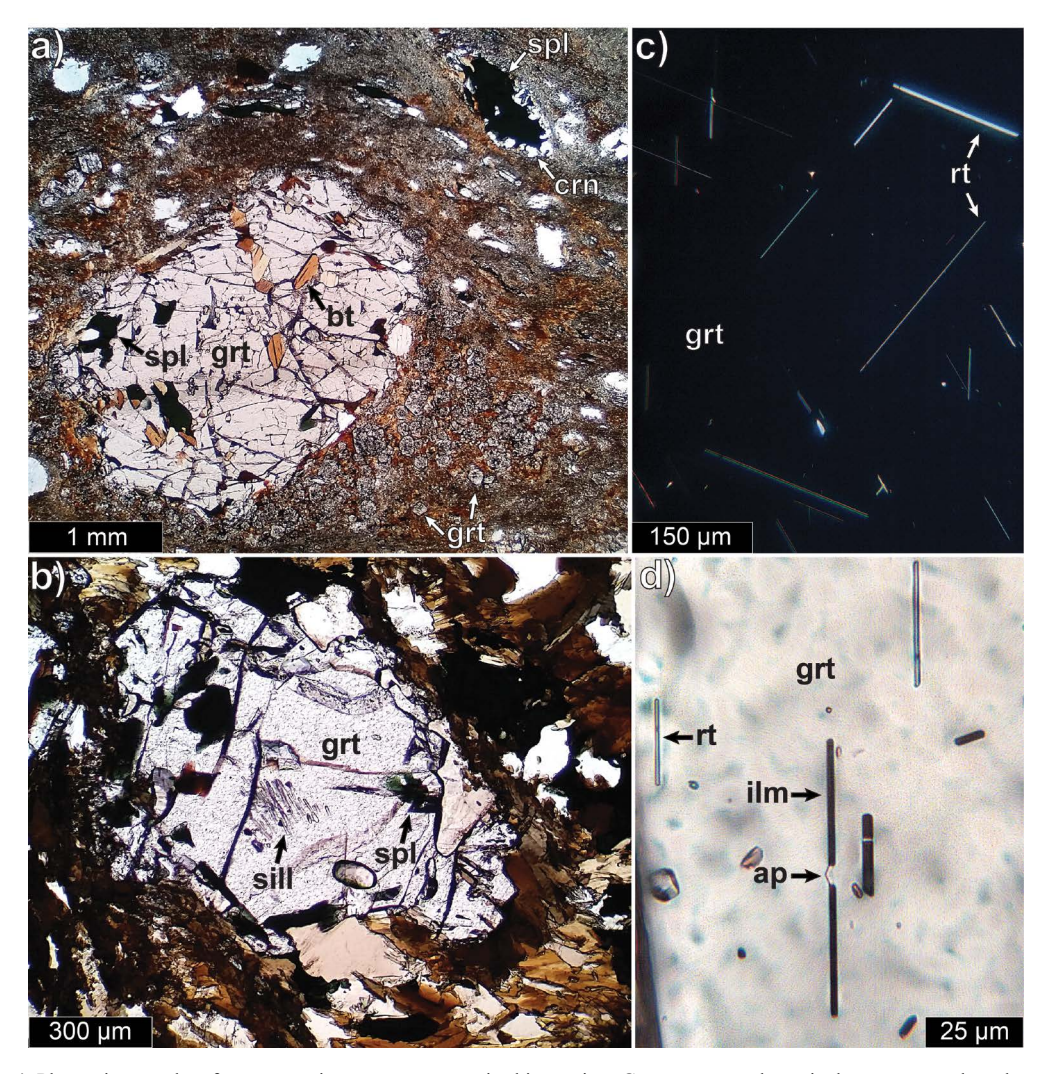


FIGURE 4. Photomicrographs of representative garnet textures in thin section. Grt = garnet, spl = spinel, crn = corundum, bt = biotite, rt = rutile, sill = sillimanite, ilm = ilmenite, ap = apatite. (a) Matrix assemblage with typical porphyroblastic garnet and second-generation euhedral garnets, as well as spinel (dark) rimmed by corundum; plane light [268A-2]. (b) Garnet with sillimanite inclusions (core) and spinel inclusions (rim) reflecting a granulite facies assemblage; plane light [296A-3]. (c) Oriented rutile needles in the core of high-phosphorus garnet (Fig. 6; Supplemental¹ Table S1), crossed polars [294A-2]. (d) Oriented rutile needles with composite needles of ilmenite and apatite in the same garnet core; plane light [294A-2]. (Color online.)

Biotite. Biotite crystals are present in both the leucosomes and the matrix and range from several millimeters across to only ~20 μm in shear bands in Type II samples. Biotite may include ilmenite and, more rarely, spinel, and is commonly included in garnet cores and rims. Representative biotite analyses are given in Supplemental¹ Table S4. Matrix biotite Mg# typically ranges from 0.35 to 0.43, in keeping with the Fe-rich bulk composition of the rock. Higher values may reflect retrograde Mg-Fe exchange with garnet. Biotite inclusions in the high-phosphorus garnet of sample 294A-1 preserve greatly elevated TiO₂ contents exceeding 6.5 wt%. Armoring by garnet may have prevented Ti loss from these biotite crystals such that they retain peak or near-peak Ti contents (see below).

Feldspar. Plagioclase is found in leucosomes, small leucocratic pockets in the matrix, and as inclusions in garnet, spinel, and biotite. Isolated matrix plagioclase grains are absent.

Antiperthite is widespread in leucosomes, but homogenous plagioclase is also found, typically adjacent to K-feldspar. The leucosomes surrounding peritectic garnet contain the antiperthites with the coarsest exsolution lamellae (Figs. 3b and 7a). Lamellae of K-feldspar ~1 mm wide in the core of the antiperthite with the coarsest lamellae (JAQ278A-1_ap3) are themselves perthitic and contain plagioclase lamellae up to ~2 µm across (Figs. 7e and 7f). Antiperthite host and lamellae compositions of coarse, unaltered grains in leucosomes, primarily surrounding garnet, are given in Supplemental¹ Tables S5 and S6.

Perthitic and homogeneous K-feldspar are found in leucosomes and as isolated matrix grains. K-feldspar crystals may contain inclusions of spinel and biotite. Some alkali feldspars show evidence of former elevated phosphorus content in the form of oriented apatite needles. These appear to be exsolved based on their sharp hexagonal cross sections, consistent spatial

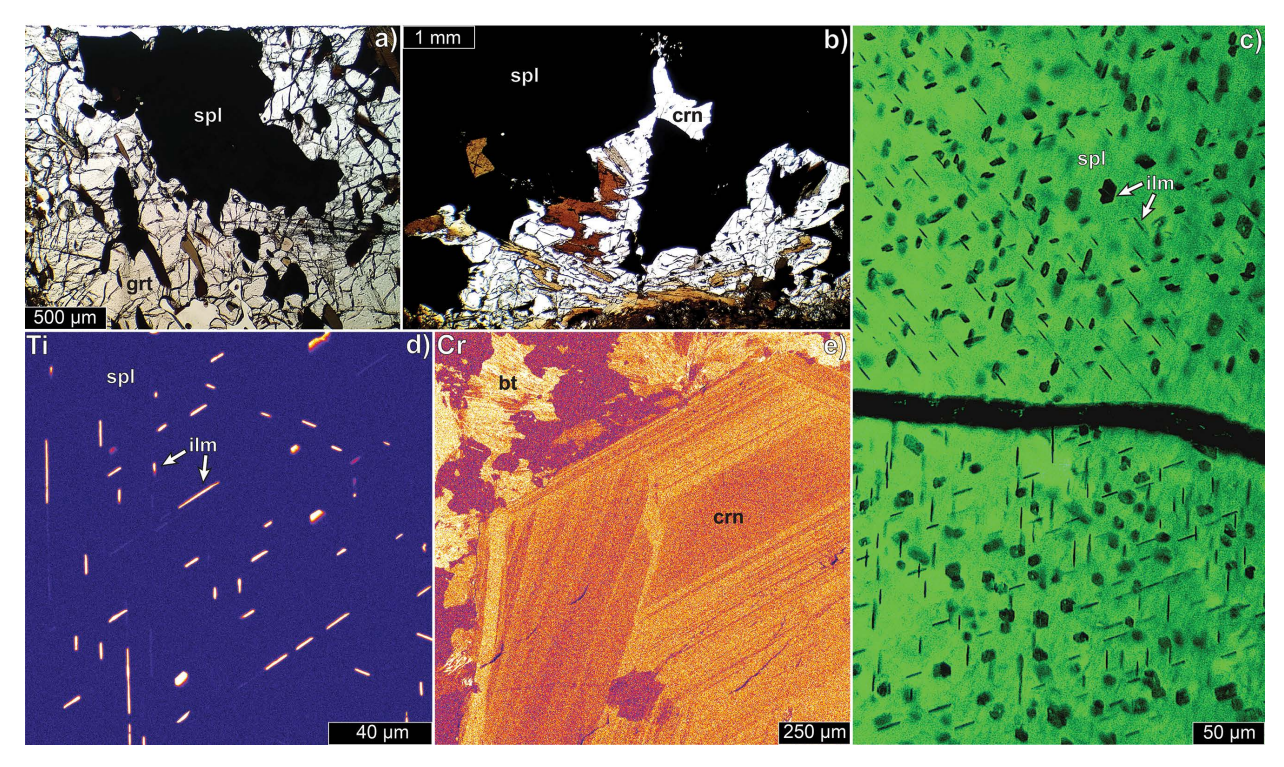


FIGURE 5. Spinel and corundum. Grt = garnet, spl = spinel, crn = corundum, ilm = ilmenite, bt = biotite. (a) Photomicrograph of ragged spinel and rounded biotite inclusions in a garnet core; plane light [296A-3]. (b) Photomicrograph of corundum with biotite inclusions cross-cutting and rimming spinel; plane light [296A-3E2]. (c) Photomicrograph (true color) of oriented Fe-Ti oxide lamellae in spinel; a domain boundary is marked by the change in lamellae orientation, condenser lens in, plane light [296A-3]. (d) Element map of Ti in spinel showing orientations of ilmenite lamellae; brighter colors indicate higher concentration [294B]. (e) Element map of Cr in a pink corundum in leucosome showing concentric euhedral growth zoning [295A-1]. (Color online.)

distribution, and alignment along crystallographic planes (Fig. 7b). Alkali feldspar with elevated phosphorus content (up to 2.5 wt%) has been reported from pegmatites and granites (e.g., London et al. 1990; London 1992; Frýda and Breiter 1995; Kontak et al. 1996); usually alkali feldspar is significantly enriched in phosphorus compared to coexisting plagioclase feldspar, either as subsolvus separate grains or hypersolvus exsolved lamellae. In Ca-poor felsic rocks, alkali feldspars contain most of the bulk-rock phosphorus because apatite is scarce (London 1992). Reintegrated perthite compositions are given in Table 2.

Antiperthites can be relict from an igneous precursor (Štípská and Powell 2005). In this study, antiperthites in metamorphic leucosomes (commonly surrounding peritectic garnet and in contact with corundum) were judged to be metamorphic, and therefore preserving solvus temperatures representative of metamorphic conditions (e.g., Figs. 3b, 7a, and 7e). The consistent distribution of antiperthites with coarse exsolution lamellae and little retrogression or resorption in leucosomes of different samples also indicates a metamorphic origin.

Perthites have several textures that indicate solid-state loss of plagioclase component. Figure 7c illustrates a typical perthite with plagioclase lamellae in the core of the grain but not in the rim. This suggests diffusional depletion of the plagioclase component into the matrix. Plagioclase blebs have a tendency to pool along cracks and grain boundaries (Fig. 7d). Plagioclase crystals adjacent to K-feldspar in leucosomes may represent lost

plagioclase component that has been recrystallized and consolidated. These characteristics suggest that the perthites do not retain their peak plagioclase content, and thus do not record peak temperatures for ternary feldspar reintegration thermometry. In contrast, antiperthites normally preserve exsolution lamellae up to their edges (Fig. 7a). Our observation that antiperthites can preserve exsolution lamellae near grain rims while perthites commonly do not has also been reported in previous studies (e.g., Zulauf et al. 2002; Hokada and Suzuki 2006).

Sillimanite. Sillimanite is found most commonly as inclusions in garnet rims, and occasionally as isolated matrix grains. Where foliation is present, sillimanite is aligned with biotite, the primary matrix mineral defining the fabric, although a later generation of sillimanite cross-cuts the foliation in some samples (Fig. 8). In a few examples, sillimanite inclusions in garnet cores form trails that may record former foliation. These cores may be relict from prograde growth or may have grown during retrogression.

Ilmenite. Ilmenite is found as discrete, subhedral grains, and as isolated and netlike masses, usually in contact with spinel and corundum. Ilmenite does not deviate far from the end-member composition, containing only minor impurities such as Si, Al, Mn, and Mg (Supplemental¹ Table S3); concentrations could have been higher, however, at peak thermal conditions. Ilmenites have low estimated Fe³⁺ contents and lack exsolution textures.

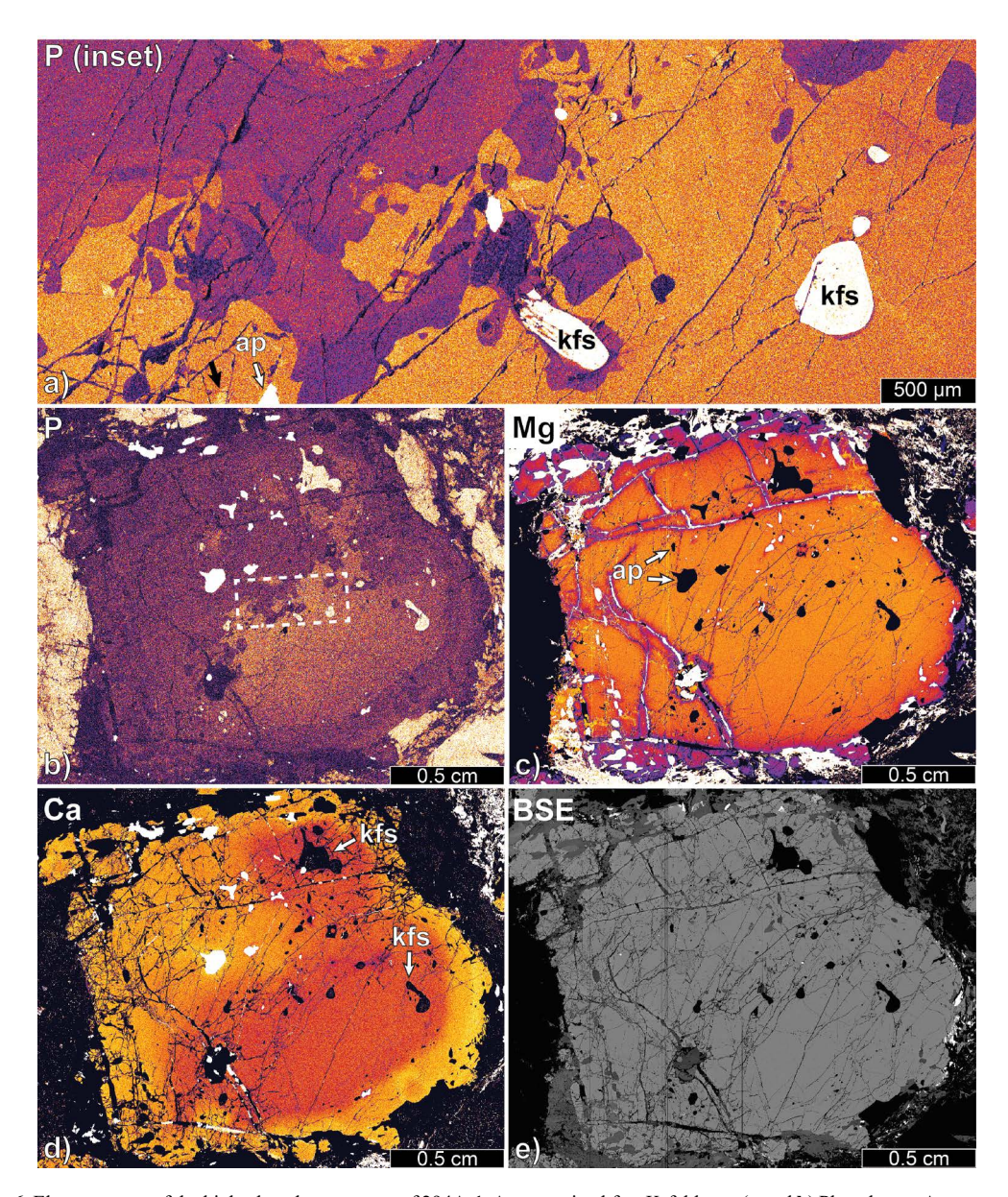


FIGURE 6. Element maps of the high-phosphorus garnet of 294A-1. Ap = apatite, kfs = K-feldspar. ($\bf a$ and $\bf b$) Phosphorus. Area mapped in detail for inset in part $\bf a$ shown as box with dashed white outline in part $\bf b$. ($\bf c$) Magnesium. ($\bf d$) Calcium. ($\bf e$) Backscattered electron image. Warmer colors indicate higher concentration. Color scale does not correlate across panels. Black arrow in inset panel $\bf a$ indicates the region with measured 0.18 wt% P_2O_5 (Supplemental Table S1). (Color online.)

Ternary feldspar reintegration thermometry

Antiperthites. The activity model of Benisek et al. (2010) returns the highest temperatures for reintegrated antiperthites, averaging 1053 ± 38 °C (2σ standard error) (Table 3; Fig. 9). The activity model of Benisek et al. (2004) yields a somewhat lower but still comparable mean of 1023 ± 20 °C (Table 3; Fig. 9). Both results use a pressure of 1.5 GPa, although the ternary feldspar solvi are only weakly pressure dependent. Regardless of activity model choice, antiperthites record T > 1000 °C (mean ~ 1040 °C); as these are solvus T estimates, they are minima. These results are in agreement with those obtained for antiperthite and mesoperthite from silicic granulites in the Brimfield Schist and Bigelow Brook

Formation (Ague et al. 2013; Axler and Ague 2015a), which gave solvus (minimum) temperatures ranging from ~900–1000 °C. Zirconium-in-rutile thermometry likewise gives T in the 1000 °C range (Ague et al. 2013), with maximum estimates of nearly 1040 °C (Axler and Ague 2015a).

Perthites. Perthite T estimates have a significant dependence on activity model, and yield means of 868 \pm 23 °C (Benisek et al. 2010) and 783 \pm 44 °C (Benisek et al. 2004) (Table 3; Fig. 9; 2σ standard error). The two activity models differ regarding the behavior of the solvus for K-feldspar-rich ternary compositions (77–85 mol%) near the K-feldspar-albite join. The perthites have textures that clearly indicate loss of plagioclase component (Figs.

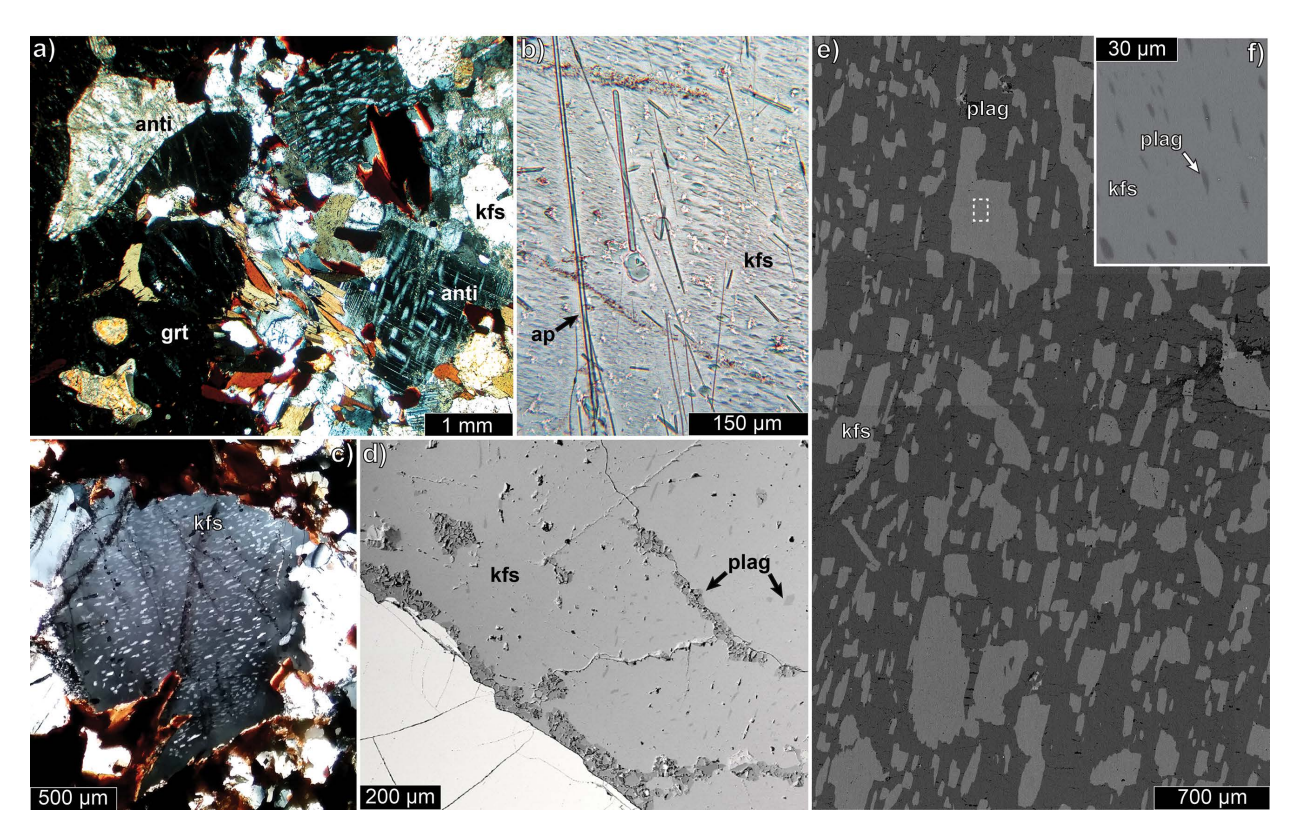


FIGURE 7. Feldspar textures. Grt = garnet, anti = antiperthite, kfs = K-feldspar, ap = apatite, plag = plagioclase. (a) Leucosome in contact with peritectic garnet [295A]. (b) Oriented apatite needles in perthite [294A-5]. (c) Perthite showing characteristic lack of exsolution lamellae in the rim, crossed polars [294A-1]. (d) Backscattered electron image of perthite (Sample T) showing plagioclase clustered along cracks and at grain boundaries [278A-1]. (e) Composite backscattered electron image of antiperthites with coarse exsolution lamellae approaching 1 mm in length [278A-1]. (f) Enlarged view of a K-feldspar lamellae in antiperthite of panel e, showing exsolution lamellae of plagioclase. (Color online.)

7c and 7d), leading to *T* estimates that are erroneously low compared to those obtained from the antiperthites, regardless of the activity model. To test this for thin section 278A-1, the perthite and coexisting grain boundary plagioclase in Figure 7d were reintegrated (Tables 3 and 4) and the solvus *T* recomputed, yielding ~915 and ~1120 °C using Benisek et al. (2004) and (2010), respectively (Table 3). These estimates are more compatible with those obtained from antiperthites.

Furthermore, we tested the assumption that this reintegrated perthite was in equilibrium with reintegrated antiperthites in the same section (278A-1, Table 3) using two-feldspar thermometry and the method of Benisek et al. (2010) (after Kroll et al. 1993, which has been applied successfully to HPG rocks such as in O'Brien et al. 1997). This method is powerful in that it corrects for retrograde Na-K resetting and requires the convergence of temperature estimates for all three feldspar end-members. Pairing the reintegrated perthite with each of the three reintegrated antiperthites in 278A-1 (Table 3) gives temperatures of 1059 °C, 1057 °C, and a non-converging, but still reasonably constrained, estimate of 1073 °C (Ab and An) to 1081 °C (Or) (Table 3). These estimates agree very well with the antiperthite results discussed above.

On this basis, we conclude that antiperthites and perthites were formerly in equilibrium before retrogression. Antiperthites mostly retained their exsolution products and, as a consequence, their reintegrated compositions yield reliable HPG solvus temperature estimates. Perthites, on the other hand, lost plagioclase component to grain boundaries and cracks. However, perthite reintegration that accounts for this lost plagioclase yields two-feldspar temperatures that are fully consistent with those from antiperthites alone.

Ti-in-biotite thermometry

We employed the Ti-in-biotite thermometer of Wu and Chen (2015) and compared its results to ternary feldspar reintegration thermometry. We used the biotite with the highest measured Ti content, which is an inclusion in the high-phosphorus garnet of sample 294A-1 (Supplemental¹ Table S4). This biotite was likely shielded from retrogression by the surrounding garnet, so as to preserve high Ti concentrations from peak thermal conditions. The thermometer gives a temperature of ~1100 °C for the average pressure of 1.8 GPa obtained from the pseudosections described below. At 1.5 GPa, the result is ~1050 °C. Although the thermometer is only calibrated for T < 840 °C, the estimates it returns agree well with the average obtained from ternary feldspar reintegration and two-feldspar thermometry.

PSEUDOSECTION MODELING

General comments

Pressure is estimated based on the phase relations for the solid phase assemblage observed in the rocks: garnet + spinel + corun-

dum + biotite + K-feldspar + ilmenite (the "full assemblage"). The phase field, which includes coexisting melt, is relatively narrow and is consistently positioned across bulk composition space, facilitating pressure estimation given constraints on temperature (Fig. 10). The field is also remarkably stable and occupies the same general position in pseudosections constructed for all three representative bulk compositions from Type I and Type II rocks. Despite differences in bulk composition among the samples, including SiO₂, Al₂O₃, K₂O, and FeO contents, the

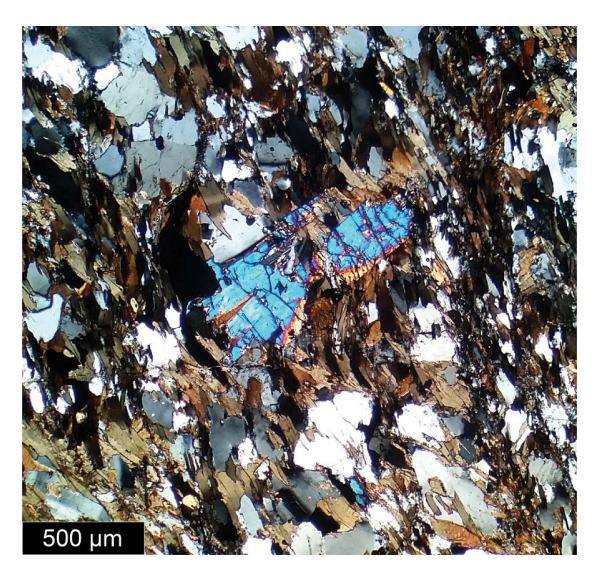


FIGURE 8. Photomicrograph of texturally late sillimanite in thin section cross-cutting foliation; crossed polars [269A-1]. (Color online.)

stability of this particular assemblage is insensitive to moderate changes in composition.

Pressure estimation

The pseudosections for samples 150A, 268A, and 269A predict equilibration at 1.65–2.1, 1.6–2.1, and 1.7–2.05 GPa, respectively, for the average reintegrated antiperthite $T \pm 2\sigma$ standard error (Fig. 10). Simultaneous spinel breakdown and corundum growth (Fig. 5b) are predicted only within the full assemblage phase field (and its lower-temperature two-feldspar

TABLE 4. Reintegrated perthite composition with grain boundary plagioclase

C	2704 1	2704 1			
Sample	278A-1 host <i>n</i> = 5	278A-1 lamellae <i>n</i> = 5			
SiO ₂	65.32(0.14)	57.60(0.46)			
Al_2O_3	18.71(0.15)	26.97(0.10)			
FeO	0.01(0.02)	0.03(0.03)			
MgO	b.d.	b.d.			
MnO	0.01(0.02)	b.d.			
CaO	0.06(0.02)	8.82(0.20)			
BaO	0.20(0.03)	0.01(0.01)			
Na₂O	1.10(0.06)	6.45(0.09)			
K ₂ O	14.96(0.11)	0.21(0.03)			
Total	100.37(0.27)	100.10(0.36)			
Structural formulas (8 0)					
Si	2.995	2.583			
Al	1.011	1.418			
Fe	0.001	0.001			
Mg					
Mn					
Ca	0.003	0.421			
Ba	0.004				
Na	0.098	0.558			
K	0.875	0.012			

 $\textit{Notes} : \text{b.d.} = \text{below detection.} \ 2\sigma \ \text{standard deviations given in parentheses.} \ \text{All Fe} \ \text{as FeO.}$

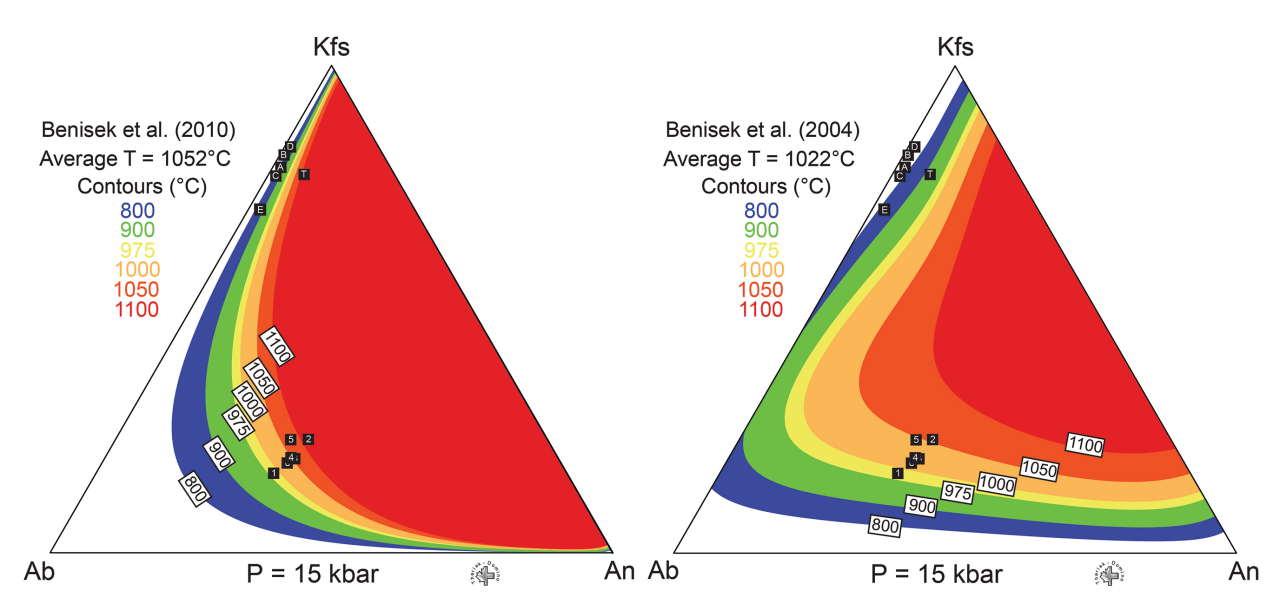


FIGURE 9. Results of ternary feldspar reintegration thermometry for antiperthites (numbers) and perthites (letters) plotted on the feldspar ternary diagram (Table 3). Temperature contours are from the feldspar activity models of Benisek et al. (2010) and Benisek et al. (2004). Sample codes 1–6 correspond to samples 150A-2, 271A-1, 278A-1 (3–5), and 281A-1, respectively. Sample codes A-F correspond to samples 294A-1 (A-C), 294A-3, and 312A-1(2×), respectively. Points E and F overlap. Points B and C come from different regions of the same grain. Point T is the perthite pictured in Figure 7d reintegrated to include grain boundary plagioclase (Tables 3 and 4). (Color online.)

extension in 150A and 269A). This texture implies that the observed assemblage formed during cooling through the full assemblage field. Ternary plagioclase is absent from this field for each sample, but this is to be expected as it is only present in leucosomes, which were intentionally excluded from bulk analyses to ensure an accurate bulk composition determination for the matrix assemblage (e.g., Guevara and Caddick 2016). For samples 150A and 269A, the down-*T*, down-*P* granulite facies two-feldspar extension of the full assemblage field predicts albite-rich plagioclase rather than significantly ternary feldspar and, thus, does not represent the observed mineralogy.

Discussion of pseudosection results

Charge balance calculations indicate Fe³⁺ in spinel, ilmenite, and garnet (Supplemental¹ Tables S1-S3). Ferric iron content estimation using ilmenite chemistry may underestimate the Fe³⁺/Fe²⁺ ratio of the bulk rock if ilmenites equilibrated in the amphibolite facies. This would not affect results significantly, as pseudosections made assuming higher Fe³⁺ content up to ~10% yield similar results. The main difference is the expansion of garnet + spinel + corundum + biotite + ilmenite + K-feldspar + melt stability for bulk compositions with more Fe³⁺. Likewise, increasing water content does not affect the results. Increasing molar H₂O by 15% produces nearly identical phase fields. Spinel has low Cr and Zn contents (Supplemental¹ Table S2). These trace elements can therefore safely be excluded from the modeling system with negligible effect on the stability range of spinel (e.g., Powell and Sandiford 1988; Shulters and Bohlen 1989; Diener and Powell 2010). Garnet and spinel, which can preserve strong chemical growth zonation, show relatively little core-to-rim variation in major or trace elements (Supplemental¹ Tables S1 and S2). The impact of prograde zonation in these modally major minerals on the accuracy of the measured effective bulk composition is therefore minimized.

In general, preservation of peak garnet compositions at ~1000 °C is unlikely because intracrystalline diffusion will be rapid (e.g., Chakraborty and Ganguly 1992; Faryad and Chakraborty 2005; Carlson 2006; Chu and Ague 2015). For example, the $2\sqrt{Dt}$ characteristic diffusive length scale for Fe in garnet at 1000 °C is several mm in 106 yr using the diffusion coefficient calibration of Chu and Ague (2015). A further complication is that isopleths of garnet Mg# and grossular content are sub-parallel across much of the modeled phase space for each sample. Moreover, ICDR has clearly affected some garnets (Fig. 6). Nonetheless, sample 150A preserves a garnet core Mg# that intersects the ternary feldspar T estimate within the full assemblage field and is closely correlated with core grossular content. The latter places minimum garnet core T equilibration at ~975 °C (Fig. 10). The analyzed garnet in sample 150A contains no plagioclase inclusions, and the rock overall has much less biotite than samples 268A and 269A; these factors may have restricted retrograde Ca and Fe-Mg exchange.

Garnet rim Mg# is consistently lower than core Mg#. Rim Mg# and grossular isopleths tend to cluster in the lower granulite facies, in some cases at lower *P* than modeled on the pseudosections. Core Mg# and grossular isopleths for sample 268A intersect at ~825 °C and ~0.6 GPa, which broadly correlates with the granulite facies overprint identified by Ague et al. (2013; 700–800 °C, 0.5–0.6 GPa) (Fig. 10). We note in this regard that garnet rims include sillimanite and rare matrix sillimanite cross-cuts foliation (Fig. 8). If the rock

remained reactive, the pseudosections predict some garnet (and sillimanite) growth during cooling through the granulite facies in the event of even a slight pressure increase following a UHT phase (Ague et al. 2013), which could account for these sillimanite textures. Sillimanite is stable for each bulk composition below ~800 °C and ~0.8 GPa. Thus, based on general isopleth trends as well as sillimanite relationships, we conclude that the granulite overprint likely affected the silica-undersaturated lithology as well.

For all three analyzed samples, pseudosections predict between 35 and 41 vol% melt at 1040 °C and 1.8 GPa. This would have decreased the strength of the rock substantially and helped facilitate the observed widespread ductile shear deformation (Fig. 2a).

Results obtained using the thermodynamic data set of Holland and Powell (1998) and compatible activity models also yield HPG pressure estimates of 1.55 to 1.7 GPa at 1040 °C. The feldspar activity model of Holland and Powell (2003) (which produces results similar to the Holland and Powell 1992 model and is standard in the Holland and Powell 2011 data set) yields reintegrated ternary feldspar temperatures >1150 °C. This places pressures as high or even higher than our preferred results (Fig. 10).

DISCUSSION

Spinel masses

The remarkable polycrystalline spinel masses documented herein deserve further comment, especially as they deviate strongly from the expected isometric spinel habit (Fig. 3c). The separation of each mass into crystallographic domains suggests that either a single cubic precursor grain underwent dynamic recrystallization, or that the grains are pseudomorphs or paramorphs after some other phase, perhaps with markedly different symmetry. As no high-pressure polymorphs of hercynitic spinel are known, we suggest that strain is responsible for recrystallizing formerly cubic spinel into an elongated, non-isometric form. Exsolution of Fe-Ti oxide could have occurred either before or after recrystallization, as each domain retained cubic symmetry (Fig. 5c). To the best of our knowledge, such large, elongated, and polycrystalline spinel forms are previously undescribed in metamorphic rocks.

The oriented Fe-Ti oxide lamellae in spinel are likely ilmenite because they contain higher Ti than the host spinel, comparable Fe, and negligible Al. Intergrowths of spinel and ilmenite have been reported from UHT granulites (e.g., Sengupta et al. 1999) although they are not oriented lamellae of one phase inside of another. Nonetheless, these features have been interpreted as resulting from the expulsion of an ülvospinel (Fe₂TiO₄) component from a precursor high-Ti spinel (Sengupta et al. 1999). Given this, and the clear crystallographic shape-preferred orientation of the lamellae, we suggest that they formed via exsolution and, thus, the Ti necessary to form the precipitates was soluble in hercynitic spinel at HPG or UHT conditions. This presupposes that the precursor phase was a spinel, but the isometric lattice constraints of the platelets suggest that they precipitated from a host phase with cubic symmetry, so spinel is the most likely candidate.

A reintegrated spinel formula shows that the precursor spinel contained 0.2 mol% ülvospinel component (277A-3; Supplemental¹ Table S2; computed following Sack and Ghiorso 1991a, 1991b). An unexsolved spinel from a different sample (294A core; Supplemental¹ Table S2) has a higher ülvospinel mol%

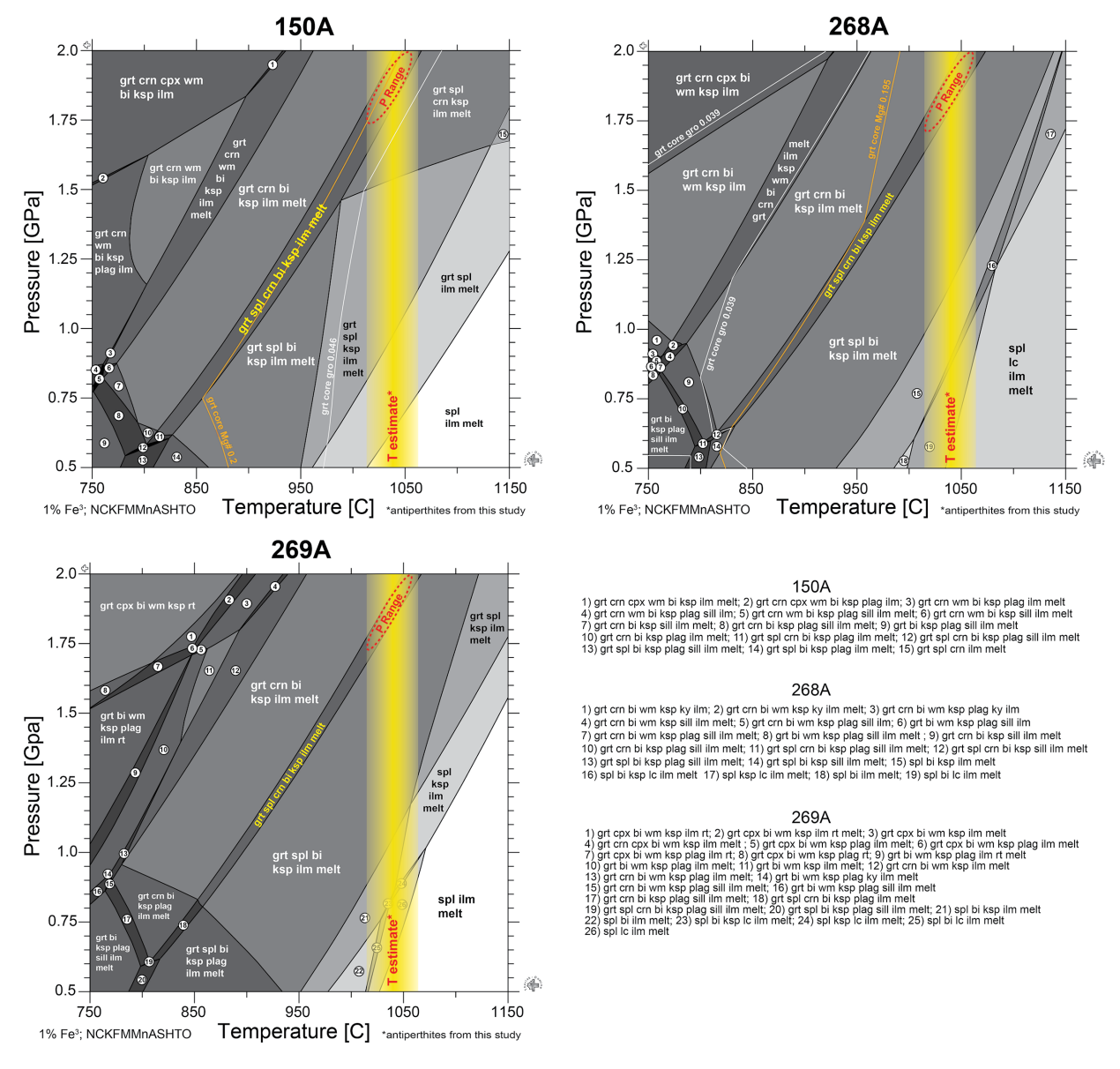


FIGURE 10. Pseudosections constructed for samples 150A, 268A, and 269A. Grt = garnet, crn = corundum, cpx = clinopyroxene, wm = white mica, bi = biotite, ksp = K-feldspar, ilm = ilmenite, plag = plagioclase, sill = sillimanite, spl = spinel, ky = kyanite, lc = leucite, rt = rutile, gro = grossular. Yellow band shows the mean $\pm 2\sigma$ standard error of the antiperthite temperatures of all analyses (Table 3) using the feldspar activity models of Benisek et al. (2004) and Benisek et al. (2010). (Color online.)

of 0.5. Other spinels in this sample show exsolution textures. Pseudosection calculations predict between 2 and 3 mol% ulvospinel component in spinel at peak conditions (1040 °C, 1.8 GPa) and ~2 mol% at UHT conditions of 900 °C and 0.9 GPa, so the spinel precursors likely equilibrated with decreased Ti content during cooling from granulite facies conditions prior to ilmenite exsolution. The spinel textures deserve further work as they may hold information about pressure and temperature conditions, melt fraction, and strain rate or magnitude.

Trace elements and ICDR in garnet

Rutile, ilmenite, and apatite lamellae in the core of the phosphorus-rich garnet of sample JAQ294A-1 are interpreted

as precipitates from a garnet richer in Ti and phosphorus stable at $T \ge 1000$ °C and $P \ge \sim 1.8$ GPa. Similar textures are present in garnet cores from silicic granulites of the Brimfield Schist and Bigelow Brook Formation (Ague and Eckert 2012; Ague et al. 2013; Axler and Ague 2015a). Given that the silica-undersaturated HPG lithology and the silicic gneisses appear to share at least a retrograde history, we expect that the amount of Ti in the precursor garnet would have been stable at HPG or UHT conditions, similar to the conclusion of Ague and Eckert (2012). Solubility of Ti in garnet is thought to be controlled more by temperature than pressure at P < 5 GPa, and although UHP majoritic substitutions may change this trend, the pressure dependence of Ti substitution in garnet is not yet clear (e.g., van

Roermund et al. 2000; Zhang et al. 2003; Ackerson et al. 2017).

Apatite precipitates have been reported from garnets in UHP rocks and kimberlite xenoliths, and phosphorus-bearing garnets have been produced at UHP conditions in laboratory studies, demonstrating that phosphorus is soluble in garnet at high pressure (Fung and Haggerty 1995; Ye et al. 2000; Mposkos and Kostopoulos 2001; Hermann and Spandler 2008; Perchuck 2008; Konzett and Frost 2009; Konzett et al. 2012; Ruiz-Cruz and Sanz de Galdeano 2013; Alifirova et al. 2015; Axler and Ague 2015b; Sakamaki et al. 2016). Garnet in the diamondiferous Saidenbachite of the Erzgebirge contains >0.3 wt% P₂O₅, and garnet in the HPG Saxony granulite has nearly 0.5 wt% (Axler and Ague 2015b; Ague and Axler 2016). Indeed, high P2O5 in garnet (0.18 to 0.22 wt%) has been used to argue for prior UHP conditions in the Acadian orogen (Snoeyenbos and Koziol 2008; Peterman et al. 2016). Experiments by Konzett (2016) on basaltic eclogites demonstrate that garnet can hold 0.17 wt% P₂O₅ at 2 GPa and 975 °C, comparable to the highest phosphorus content we have measured (0.18 wt% P₂O₅; Supplemental¹ Table S1). Thus, although UHP conditions may not be required to produce the phosphorus levels we observe, the Konzett (2016) experiments strongly suggest that the P-T conditions recorded by the silica-undersaturated rocks are nonetheless unusual for crustal metamorphism.

The striking ICDR record preserved by irregular phosphorus zoning in garnet (Fig. 6a) has many parallels to that found in garnet from the HPG Saxony Granulite (Ague and Axler 2016). In both samples, phosphorus zonation is highly irregular and shows little diffusional smoothing. In the CT HPG sample, "cutout" depletion halos around K-feldspar inclusions reveal that the inclusion-host interface may provide an expedited fluid pathway, enabling ICDR reactions to penetrate more efficiently in more poikiloblastic grains. Partial diffusional smoothing of Ca and total smoothing of Mg provide further evidence that phosphorus diffuses more slowly than major elements in garnet, making it a valuable recorder of growth zonation and later modifications (e.g., Ague and Axler 2016). Fluid infiltration at HPG, granulite, or amphibolite-facies conditions could have produced the observed ICDR zonation. Further research is required to understand the extent to which ICDR may be responsible for modifying mineral compositions in high-grade rocks, especially how to distinguish fluid signatures from melt signatures.

Petrogenesis

Thermometry and pseudosection modeling place equilibration of the silica-undersaturated HPG lithology in the HPG realm at ~1040 °C and ~1.8 GPa. This pressure requires exhumation from a depth of ~60 km (assuming lithostatic pressure) and thus either burial to the base of orogenically thickened continental crust or thermal equilibration during exhumation from a hot subduction zone. Both of these scenarios have been proposed for high-pressure granulites (O'Brien and Rötzler 2003; O'Brien 2008). Eclogite facies rocks are thought to become high-pressure granulites during exhumation in some cases (e.g., Willner et al. 1997; Yao et al. 2000; Zhao et al. 2001; O'Brien and Rötzler 2003; Kim et al. 2006; Nahodilová et al. 2011). Marschall et al. (2003) suggested that Variscan granulites from the Schwarzwald were heated by basaltic magmas at the base of the orogenic belt

and subsequently exhumed by orogenic extension. High levels of mantle heat input have also been invoked to explain high-*T* Variscan metamorphism (Sorger et al. 2018). Another possible parallel is the Gruf Complex of the Alps, which may have been heated to its UHT conditions by mantle diapirs (e.g., Galli et al. 2011). We conclude that the presence of HPG rocks in the CMT imposes new constraints on metamorphism and tectonism, namely that the thrust sheets of the southern CMT must have sampled the orogenic root and/or deeper settings during the assembly of composite Laurentia.

If the rocks formed in a subduction environment, their provenance is a hint that Acadian-Neoacadian terranes may hold similarly deeply subducted rocks to those known from contiguous Caledonian terranes in Greenland and Europe, which contain HPGs as well as the second-largest UHP terrane (by geographic extent) (Gilotti and Elvevold 2002; Gilotti and Krogh Ravna 2002; Hacker et al. 2010; Gilotti 2013; Klonowska et al. 2017). Some Acadian rocks have already been suggested as being indicative of deep subduction (e.g., Peterman et al. 2016).

IMPLICATIONS FOR SYENITES AND ALUMINOUS XENOLITHS

Our model of the high-pressure metamorphism and partial melting that produced leucosomes within the silica-undersaturated granulite of the CMT has implications for both syenite genesis and the origins of highly aluminous xenoliths.

Leucosomes in the silica-undersaturated rocks, which were likely generated in situ, are effectively syenites consisting of two feldspars and biotite. Notably, syenite bodies with younger crystallization ages than peak metamorphic conditions are reported from several UHT terranes (e.g., Brandt et al. 2003; Karmakar and Schenk 2016) and some UHT localities have syenitic leucosomes (e.g., Hokada and Harley 2004). Moreover, lower-crustal UHT and HPG metapelites have been explicitly considered as syenite producers (e.g., Litvinovsky et al. 2000, 2002; Tchameni et al. 2001; Hacker et al. 2005; Shaffer et al. 2017). Nonetheless, the prevailing consensus is that some mantle input is responsible for many syenite provinces (e.g., Harris et al. 1983; Bailey 1987; Kramm and Kogarko 1994; Litvinovsky et al. 2002; Markl et al. 2010) and some syenite bodies have strong petrological evidence for mantle melt participation (e.g., Lang et al. 1995), such as zoned syenite-pyroxenite dikes. Laboratory results showing that syenites can be produced by HPG silicic rocks offer compelling evidence that high-grade aluminous rocks like the silica-undersaturated rocks of this study may also produce syenites (Litvinovsky et al. 2000).

The density of the CT silica-undersaturated HPGs may provide a key clue to an aspect of syenite genesis and possibly also delamination. Delamination of the lower crust or lithospheric mantle has been the focus of much previous work (e.g., Bird 1978, 1979; Houseman et al. 1981; Rudnick 1995; Zegers and van Keken 2001; Anderson 2005) and delamination has been suggested to follow alkaline igneous melt generation in lower crustal domains (Smithies and Champion 1999). We suggest that the silica-undersaturated high-pressure granulite in the CMT was a syenite source that did not melt to its full extent and delaminate.

Densities of the samples were calculated using Theriak-

Domino (Table 1). At 1040 °C and 1.8 GPa their average density is 3.0 g/cm³, which is roughly as dense as basalt and significantly denser than molten basalt (Ahrens and Johnson 1995). If 50% of the melt calculated to be present at these *P-T* conditions was extracted from the rock, density would increase to 3.0–3.2 g/cm³, which is near that of the peridotitic or dunitic mantle (Daly et al. 1966; Boyd and McCallister 1976; Rudnick 1995). If all of the melt was extracted (with no more being generated), densities would reach 3.2–3.5 g/cm³, roughly as dense as eclogite, which is negatively buoyant relative to aesthenospheric mantle (Ahrens and Johnson 1995; Rudnick 1995; Zegers and van Keken 2001). If more melting and melt loss occurred beyond what the CT rocks underwent, then density would be driven even higher as more feldspar and biotite are lost.

Depending on the mantle rock type directly beneath the base of the orogenic crust, and the degree to which that part of the mantle wedge was hydrated, delamination might release the aluminous rock into the mantle (e.g., Hacker et al. 2011). Delamination could be triggered by buoyant upwelling of magma pooling at the base of the crust or by crustal flow in response to orogenic deformation (e.g., Bird 1978; Houseman et al. 1981). If delamination followed melt generation and loss, the syenite source region would founder into the mantle, leaving only the released melt within the crust.

We recognize that there are likely many complex aspects to syenite generation and that no one model is likely to account for the varied settings in which syenites are found. Further study of syenites in terranes with anatectic UHT/HPG metapelites may well reveal that these magmas can be generated at the base of orogenically thickened crust or in rift zones. Rocks like those of this study may satisfy the requirements of "missing" syenite source regions both chemically and physically.

Melt removal also has implications for the origins of highly aluminous xenoliths in kimberlites containing various combinations of garnet, spinel, and corundum (e.g., Nixon et al. 1978; Padovani and Tracy 1981; Exley et al. 1983; Mazzone and Haggerty 1989). Pseudosections (Fig. 10) show that large degrees of partial melting and melt removal would leave behind highly aluminous restites enriched in garnet + spinel ± corundum (+ ilmenite) that would bear strong mineralogical similarities to the kimberlite xenoliths. As discussed above, if the restites reside at the base of the crust and are dense enough, they could delaminate and founder into the mantle. They would then be available to become entrained in kimberlites. Alternatively, such residues might also form by extreme melt loss from metasediments in subducted slabs, prior to incorporation in kimberlites (e.g., Mazzone and Haggerty 1989). This melt loss would, in turn, release syenitic melts and associated fluids to arc magma source regions. Either scenario is broadly compatible with current hypotheses for HPG genesis at the base of orogenically thickened crust or as a consequence of "hot" subduction zone activity (e.g., O'Brien and Rötzler 2003; Marschall et al. 2003; O'Brien 2008). Delamination or subduction would help to explain the relatively uncommon occurrence of these rocks in exhumed orogenic belts.

ACKNOWLEDGMENTS

We thank E.M. Stewart, J.A. Axler, S. Fererro, D.M. Rye, M.T. Brandon, and J.B. Murphy for discussions, J.O. Eckert Jr. for his EPMA expertise, M. Caddick, J.A.D. Connolly, and D.K. Tinkham for help with the HP11 database, and S. Ni-

colescu and F. Phillips for photography assistance. We also thank B.R. Hacker and C.A. Hauzenberger for thorough and constructive reviews. Becker Construction Company graciously allowed access to the field area. Support from the National Science Foundation (EAR-0744154, EAR-1250269, and EAR-1753553) and Yale University is gratefully acknowledged.

REFERENCES CITED

- Ackerson, M.R., Watson, E.B., Tailby, N.D., and Spear, F.S. (2017) Experimental investigation into the substitution mechanisms and solubility of Ti in garnet. American Mineralogist, 102, 158–172.
- Ague, J.J. (1995) Deep crustal growth of quartz, kyanite and garnet into large-aperture, fluid-filled fractures, north-eastern Connecticut, USA. Journal of Metamorphic Geology, 13, 299–314.
- —— (2011) Extreme channelization of fluid and the problem of element mobility during Barrovian metamorphism. American Mineralogist, 96, 333–352.
- Ague, J.J., and Axler, J.A. (2016) Interface coupled dissolution-reprecipitation in garnet from subducted granulites and ultrahigh-pressure rocks revealed by phosphorous, sodium, and titanium zonation. American Mineralogist, 101, 1696–1699.
- Ague, J.J., and Eckert, J.O. Jr. (2012) Precipitation of rutile and ilmenite needles in garnet: Implications for extreme metamorphic conditions in the Acadian Orogen, U.S.A. American Mineralogist, 840–855.
- Ague, J.J., Eckert, J.O. Jr., Chu, X., Baxter, E.F., and Chamberlain, C.P. (2013) Discovery of ultrahigh-temperature metamorphism in the Acadian orogen, Connecticut, USA. Geology, 41, 271–274.
- Ahrens, T.J., and Johnson, M.L. (1995) Shock Wave Data for Rocks. In T. J. Ahrens Ed., Rock Physics & Phase Relations: A Handbook of Physical Constants pp. 35-44. American Geophysical Union, Washington, D.C.
- Aleinikoff, J.N., Wintsch, R.P., Tollo, R.P., Unruh, D.M., Fanning, C.M., and Schmitz, M.D. (2007) Ages and origins of rocks of the Killingworth dome, south-central Connecticut: implications for the tectonic evolution of southern New England. American Journal of Science, 307, 63–118.
- Alifirova, T.A., Pokhilenko, L.N., and Korsakov, A.V. (2015) Apatite, SiO₂, rutile and orthopyroxene precipitates in minerals of eclogite xenoliths from Yakutian kimberlites, Russia. Lithos, 226, 31-49.
- Anderson, D.L. (2005) Large igneous provinces, delamination, and fertile mantle. Elements, 1, 271–275.
- Armstrong, T.R., Tracy, R.J., and Hames, W.E. (1992) Contrasting styles of Taconian, Eastern Acadian and Western Acadian metamorphism, central and western New England. Journal of Metamorphic Geology, 10, 415–426.
- Asami, M., Makimoto, H., and Grew, E.S. (1989) Geology of the Eastern Sør Rondane Mountains, East Antarctica. Proceedings of the National Institute of Polar Research Symposium on Antarctic Geoscience. 3, 81–99.
- Asami, M., Grew, E.S., and Makimoto, H. (1990) A staurolite-bearing corundum-garnet gneiss from the Eastern Sør Rondane Mountains, Antarctica. Proceedings of the National Institute of Polar Research Symposium on Antarctic Geoscience. 4, 22–40.
- Axler, J.A., and Ague, J.J. (2015a) Oriented multiphase needles in garnet from ultrahigh-temperature granulites, Connecticut, U.S.A. American Mineralogist, 100, 2254–2271.
- ——— (2015b) Exsolution of rutile or apatite precipitates surrounding ruptured inclusions in garnet from UHT and UHP rocks. Journal of Metamorphic Geology, 33, 829–848.
- (2015c) Too hot for zircons? U-Pb zircon geochronology of the ultrahigh-temperature (UHT) region of the Central Maine Terrane, Connecticut, USA. Geological Society of America Abstracts with Programs, 47, 773.
- Bailey, D.K. (1987) Mantle metasomatism—perspective and prospect. In J.G. Fitton and B.G.J. Upton, Eds., Alkaline Igneous Rocks, Geological Society, London, Special Publications, 30, 1–13.
- Baldwin, J.A., Bowring, S.A., and Williams, M.L. (2003) Petrological and geochronological constraints on high pressure, high temperature metamorphism in the Snowbird tectonic zone, Canada. Journal of Metamorphic Geology, 21, 81–208
- Barker, F. (1964) Reaction between mafic magmas and pelitic schist, Cortlandt, New York. American Journal of Science, 262, 614–634.
- Benisek, A., Kroll, H., and Cemič, L. (2004) New developments in two-feldspar thermometry. American Mineralogist, 89, 1496–1504.
- Benisek, A., Dachs, E., and Kroll, H. (2010) A ternary feldspar-mixing model based on calorimetric data: development and application. Contributions to Mineralogy and Petrology, 160, 327–337.
- Bird, P. (1978) Initiation of intracontinental subduction in the Himalaya. Journal of Geophysical Research, 83, 4975–4987.
- ——— (1979) Continental Delamination and the Colorado Plateau. Journal of Geophysical Research, 84, 7561–7571.
- Boyd, F.R., and McCallister, R.H. (1976) Densities of fertile and sterile garnet peridotites. Geophysical Research Letters, 3, 509–512.
- Brandt, S., Klemd, R., and Okrusch, M. (2003) Ultrahigh-temperature metamorphism and multistage evolution of garnet-orthopyroxene granulites from the Proterozoic Epupa Complex, NW Namibia. Journal of Petrology, 44,

- 1121-1144.
- Brown, M. (2006) Duality of thermal regimes is the distinctive characteristic of plate tectonics since the Neoarchean. Geology, 34, 961–964.
- Carlson, W.D. (2006) Rates of Fe, Mg, Mn, and Ca diffusion in garnet. American Mineralogist, 91, 1–11.
- Chakraborty, S., and Ganguly, J. (1992) Cation diffusion in aluminosilicate garnets: experimental determination in spessartine-almandine diffusion couples, evaluation of effective binary diffusion coefficients, and applications. Contributions to Mineralogy and Petrology, 111, 74–86.
- Chamberlain, C.P., and England, P.C. (1985) The Acadian thermal history of the Merrimack Synclinorium in New Hampshire. The Journal of Geology, 93, 593–602
- Chu, X., and Ague, J.J. (2015) Analysis of experimental data on divalent cation diffusion kinetics in aluminosilicate garnets with application to timescales of peak Barrovian metamorphism, Scotland. Contributions to Mineralogy and Petrology, 170, 25.
- Clifford, T.N., Stumpfl, E.F., and McIver, J.R. (1975) A sapphirine-cordierite-bronzite-phlogopite paragenesis from Namaqualand, South Africa. Mineralogical Magazine, 40, 347–356.
- Daly, R.A., Manger, G.E., and Clark, S.P. Jr. (1966) Density of rocks. In S.P. Clark Jr., Ed., Handbook of Physical Constants—Revised Edition. Geological Society of America Memoir, 97, 19–26.
- De Capitani, C., and Petrakakis, K. (2010) The computation of equilibrium assemblage diagrams with Theriak/Domino software. American Mineralogist, 95, 1006–1016.
- Dharmapriya, P.L., Malaviarachchi, S.P.K., Galli, A., Su, B., Subasinghe, N.D., and Dissanayake, C.B. (2015) Rare evidence for formation of garnet + corundum during isobaric cooling of ultrahigh temperature metapelites: New insights for retrograde *P-T* trajectory of the Highland Complex, Sri Lanka. Lithos, 220-223, 300–317.
- Diener, J.F.A., and Powell, R. (2010) Influence of ferric iron on the stability of mineral assemblages. Journal of Metamorphic Geology, 28, 599–613.
- Dorfler, K.M., Tracy, R.J., and Caddick, M.J. (2014) Late-stage orogenic loading revealed by contact metamorphism in the northern Appalachians, New York. Journal of Metamorphic Geology, 32, 113–132.
- Dorfler, K.M., Caddick, M.J., and Tracy, R.J. (2015) Thermodynamic modeling of crustal melting using xenolith analogs from the Cortlandt Complex, New York, USA. Journal of Petrology, 56, 389–408.
- Exley, R.A., Smith, J.V., and Dawson, J.B. (1983) Alkremite, garnetite, and eclogite xenoliths from Bellsbank and Jagersfontein, South Africa. American Mineralogist, 68, 512–516.
- Fahey, R.J., and Pease, M.H. Jr. (1977) Preliminary bedrock geologic map of the South Coventry quadrangle, Tolland County, Connecticut. U.S. Geological Survey Open-File Report, 77-587.
- Faryad, S.W., and Chakraborty, S. (2005) Duration of Eo-Alpine metamorphic events obtained from multicomponent diffusion modeling of garnet: a case study from the Eastern Alps. Contributions to Mineralogy and Petrology, 150, 306–318.
- Ferrero, S., Axler, J., Ague, J.J., Wunder, B., and Ziemann, M.A. (2017) Preserved anatectic melt in ultrahigh-temperature (or high pressure?) felsic granulites, Connecticut, US. Geophysical Research Abstracts, 19, EGU2017-9692-1.
- Frýda, J., and Breiter, K. (1995) Alkali feldspars as a main phosphorus reservoirs in rare-metal granites: three examples from the Bohemian Massif (Czech Republic). Terra Nova, 7, 315–320.
- Fung, A.T., and Haggerty, S.E. (1995) Petrography and mineral compositions of eclogites from the Koidu Kimberlite Complex, Sierra Leone. Journal of Geophysical Research, 100, 20451–20473.
- Galli, A., Le Bayon, B., Schmidt, M.W., Burg, J-P., Caddick, M.J., and Reusser, E. (2011) Granulites and charnockites of the Gruf Complex: Evidence for Permian ultra-high temperature metamorphism in the Central Alps. Lithos, 124, 17–45.
- Getty, S.R., and Gromet, L.P. (1992) Geochronological constraints on ductile deformation, crustal extension, and doming about a basement-cover boundary, New England Appalachians. American Journal of Science, 292, 359–397, doi: 10.2475/ajs.292.6.359.
- Gilotti, J. (2013) The realm of ultrahigh-pressure metamorphism. Elements, 9, 255–260.
- Gilotti, J.A., and Elvevold, S. (2002) Extensional exhumation of a high-pressure granulite terrane in Payer Land, Greenland Caledonides: structural, petrologic, and geochronologic evidence from metapelites. Canadian Journal of Earth Science, 39, 1169–1187.
- Gilotti, J.A., and Krogh Ravna, E.J. (2002) First evidence for ultrahigh-pressure metamorphism in the North-East Greenland Caledonides. Geology, 30, 551-554.
- Grant, J.A. (1985a) Phase equilibria in low-pressure partial melting of pelitic rocks. American Journal of Science, 285, 409–435.
- ———(1985b) Phase equilibria in partial melting of pelitic rocks. In J.R. Ashworth Ed., Migmatites, pp. 86–144. Chapman and Hall.
- Griffin, W.L., Jensen, B.B., and Misra, S.N. (1971) Anomalously elongated rutile in eclogite-facies pyroxene and garnet. Norsk Geologisk Tidsskrift, 51, 177–185. Guevara, V., and Caddick, M. (2016) Shooting at a moving target: Phase equilib-

- ria modelling of high-temperature metamorphism. Journal of Metamorphic Geology, 34, 209–235.
- Hacker, B.R., Luffi, P., Lutkov, V., Minaev, V., Ratschbacher, L., Plank, T., Ducea, M., Patiño-Douce, A., McWilliams, M., and Metcalf, J. (2005) Near-ultrahigh pressure processing of continental crust: Miocene crustal xenoliths from the Pamir. Journal of Petrology, 46, 1661–1687.
- Hacker, B.R., Andersen, T.B., Johnston, S., Kylander-Clark, A.R.C., Peterman, E.M., Walsh, E.O., and Young, D. (2010) High-temperature deformation during continental-margin subduction & exhumation: The ultrahigh-pressure Western Gneiss Region of Norway. Tectonophysics, 480, 149–171.
- Hacker, B.R., Kelemen, P.B., and Behn, M.D. (2011) Differentiation of the continental crust by relamination. Earth and Planetary Science Letters, 307, 501–516.
- Harley, S.L. (1998) On the occurrence and characterization of ultrahigh-temperature crustal metamorphism. In P.J. Treloar and P.J. O'Brien, Eds., What Drives Metamorphism and Metamorphic Reactions? Geological Society, London, Special Publications, 138, 81–107.
- Harlov, D.E., Wirth, R., and Hetherington, C.J. (2011) Fluid-mediated partial alteration in monazite: the role of coupled dissolution-reprecipitation in element redistribution and mass transfer. Contributions to Mineralogy and Petrology, 162, 329–348.
- Harris, N. (1981) The application of spinel-bearing metapelites to P/T determinations: An example from South India. Contributions to Mineralogy and Petrology, 76, 229–233.
- Harris, N.B.W., Duyverman, H.J., and Almond, D.C. (1983) The trace element and isotope geochemistry of the Sabaloka Igneous Complex, Sudan. Journal of the Geological Society of London, 140, 245–256.
- Hermann, J., and Spandler, C.J. (2008) Sediment melts at sub-arc depths: an experimental study. Journal of Petrology, 49, 717–740.
- Hibbard, J.P., van Staal, C.R., Rankin, D.R., and Williams, H. (2006) Lithotectonic map of the Appalachian orogen, Canada-United States of America, scale 1:1,500,000. Geological Survey of Canada.
- Hokada, T., and Harley, S. (2004) Zircon growth in UHT leucosome: constraints from zircon-garnet rare earth elements (REE) relations in Napier Complex, East Antarctica. Journal of Mineralogical and Petrological Sciences, 99, 180–190.
- Hokada, T., and Suzuki, S. (2006) Feldspar in felsic orthogneiss as indicator for UHT crustal processes. Journal of Mineralogical and Petrological Sciences, 101, 260–264.
- Holland, T., and Powell, R. (1992) Plagioclase feldspars: Activity-composition relations based upon Darken's quadratic formalism and Landau theory. American Mineralogist, 77, 53–61.
- (1996) Thermodynamics of order-disorder in minerals: II. Symmetric formalism applied to solid solutions. American Mineralogist, 81, 1425–1437.
- ——— (1998) An internally consistent thermodynamic data set for phases of petrological interest. Journal of Metamorphic Geology, 16, 309–343.
- (2003) Activity-composition relations for phases in petrological calculations: an asymmetric multicomponent formulation. Contributions to Mineralogy and Petrology, 145, 492–501.
- ———— (2011) An improved and extended internally consistent thermodynamic dataset for phases of petrological interest, involving a new equation of state for solids. Journal of Metamorphic Geology, 29, 333–383.
- Houseman, G.A., McKenzie, D.P., and Molnar, P. (1981) Convective instability of a thickened boundary layer and its relevance for the thermal evolution of continental convergent belts. Journal of Geophysical Research, 86, 6115–6132.
- Indares, A. (1993) Eclogitized gabbros from the eastern Grenville Province: Textures, metamorphic context, and implications. Canadian Journal of Earth Sciences, 30, 159–173.
- ——(1995) Metamorphic interpretation of high-pressure-temperature metapelites with preserved growth zoning in garnet, eastern Grenville Province, Canadian Shield. Journal of Metamorphic Geology, 13, 475–486.
- ——— (1997) Garnet-kyanite clinopyroxenites and garnet-kyanite restites from the Manicouagan Imbricate Zone: a case of high-P-high-T metamorphism in the Grenville Province. Canadian Mineralogist, 35, 1161–1171.
- Indares, A., and Dunning, G. (2001) Partial melting of High-P-T metapelites from the Tshenukutish Terrane (Grenville Province): Petrography and U-Pb geochronology. Journal of Petrology, 42, 1547–1565.
- Indares, A., Dunning, G., Cox, R., Gale, D., and Connelly, J. (1998) High-pressure, high-temperature rocks from the base of thick continental crust: Geology and age constraints from the Manicouagan Imbricate Zone, eastern Grenville Province. Tectonics, 17, 426–440.
- Karmakar, S., and Schenk, V. (2016) Mesoproterozoic UHT metamorphism in the Southern Irumide Belt, Chipata, Zambia: Petrology and in-situ monazite dating. Precambrian Research, 275, 332–356.
- Kelsey, D.E. (2008) On ultrahigh-temperature crustal metamorphism. Gondwana Research, 13, 1–29.
- Kelsey, D.E., White, R.W., and Powell, R. (2005) Calculated phase equilibria in K₂O-FeO-MgO-Al₂O₃-SiO₂-H₂O for silica-undersaturated sapphirine-bearing mineral assemblages. Journal of Metamorphic Geology, 23, 217–239.
- Kim, S.W., Oh, C.W., Williams, I.S., Rubatto, D., Ryu, I., Rajesh, V.J., Kim, C., Guo, J., and Zhai, M. (2006) Phanerozoic high-pressure eclogite and intermediate-pressure granulite facies metamorphism in the Gyeonggi Massif, South

- Korea: Implications for the eastward extension of the Dabie-Sulu continental collision zone. Lithos, 92, 357–377.
- Klonowska, I., Janák, M., Majka, J., Petrík, I., Froitzheim, N., Gee, D.G., and Sasinkova, V. (2017) Microdiamond on Åreskutan confirms regional UHP metamorphism in the Seve Nappe Complex of the Scandanavian Caledonides. Journal of Metamorphic Geology, 35, 541–564.
- Kontak, D.J., Martin, R.F., and Richard, L. (1996) Patterns of phosphorus enrichment in alkali feldspar, South Mountain Batholith, Nova Scotia, Canada. European Journal of Mineralogy, 8, 805–824.
- Konzett, J. (2016) From phosphates to silicates and back: An experimental study on the transport and storage of phosphorus in eclogites during uplift and exhumation. American Mineralogist, 101, 1756–1768.
- Konzett, J., and Frost, D.J. (2009) The High P-T stability of hydroxyl-apatite in natural and simplified MORB-an experimental study to 15 GPa with implications for transport and storage of phosphorus and halogens in subduction zones. Journal of Petrology, 50, 2043–2062.
- Konzett, J., Rhede, D., and Frost, D.J. (2012) The high PT stability of apatite and Cl partitioning between apatite and hydrous potassic phases in peridotite: an experimental study to 19 GPa with implications for the transport of P, Cl and K in the upper mantle. Contributions to Mineralogy and Petrology, 163, 277–296.
- Kotková, J. (2007) High-pressure granulites of the Bohemian Massif: recent advances and open questions. Journal of Geosciences, 52, 45–71.
- Kramm, U., and Kogarko, L.N. (1994) Nd and Sr isotope signatures of the Khibina and Lovozero agpaitic centres, Kola Alkaline Province, Russia. Lithos, 32, 225–242.
- Kroll, H., Evangelakakis, C., and Voll, G. (1993) Two-feldspar geothermometry: a review and revision for slowly-cooled rocks. Contributions to Mineralogy and Petrology, 114, 510–518.
- Lal, R.K., Ackermand, D., Seifert, F., and Haldar, S.K. (1978) Chemographic Relationships in Sapphirine-Bearing Rocks From Sonapahar, Assam, India. Contributions to Mineralogy and Petrology, 67, 169–187.
- Lang, J.R., Lueck, B., Mortensen, J.K., Russell, J.K., Stanley, C.R., and Thompson, J.F.H. (1995) Triassic-Jurassic silica-undersaturated and silica-saturated alkalic intrusions in the Cordillera of British Columbia: Implications for arc magmatism. Geology, 23, 451–454.
- Litvinovsky, B.A., Steele, I.M., and Wickham, S.M. (2000) Silicic magma formation in overthickened crust: melting of charnockite and leucogranite at 15, 20 and 25 kbar. Journal of Petrology, 41, 717–737.
- Litvinovsky, B.A., Jahn, B., Zanvilevich, A.N., Saunders, A., Poulain, S., Kuzmin, D.V., Reichow, M.K., and Titov, A.V. (2002) Petrogenesis of syenite-granite suites from the Bryansky Complex (Transbaikalia, Russia): implications for the origin of A-type granitoid magmas. Chemical Geology, 189, 105–133.
- London, D. (1992) Phosphorus in S-type magmas: The P₂O₅ content of feldspars from peraluminous granites, pegmatites, and rhyolites. American Mineralogist, 77, 126–145.
- London, D., Černý, P., Loomis, J.L., and Pan, J.J. (1990) Phosphorus in alkali feld-spars of rare-element granitic pegmatites. Canadian Mineralogist, 28, 771–786.
- Markl, G., Marks, M.A.W., and Frost, B.R. (2010) On the controls of oxygen fugacity in the generation and crystallization of peralkaline melts. Journal of Petrology, 51, 1831–1847.
- Marschall, H.R., Kalt, A., and Hanel, M. (2003) P–T evolution of a variscan lower-crustal segment: a study of granulites from the Schwarzwald, Germany. Journal of Petrology, 44, 227–253.
- Massey, M.A., Moecher, D.P., Walker, T.B., O'Brien, T.M., and Rohrer, L.P. (2017) The role and extent of dextral transpression and lateral escape on the post-Acadian tectonic evolution of south-central New England. American Journal of Science, 317, 34–94.
- Mazzone, P., and Haggerty, S.E. (1989) Peraluminous xenoliths in kimberlite: Metamorphosed restites produced by partial melting of pelites. Geochimica et Cosmochimica Acta, 53, 1551–1561.
- Mposkos, E.D., and Kostopoulos, D.K. (2001) Diamond, former coesite and supersilicic garnet in metasedimentary rocks from the Greek Rhodope: a new ultrahigh-pressure metamorphic province established. Earth and Planetary Science Letters, 192, 497–506.
- Müller, T., Massonne, H.J., and Willner, A.P. (2015) Timescales of exhumation and cooling inferred by kinetic modeling: An example using a lamellar garnet pyroxenite from the Variscan Granulitgebirge, Germany. American Mineralogist, 100, 747–759.
- Nahodilová, R., Faryad, S.W., Dolejš, D., Tropper, P., and Konzett, J. (2011) High-pressure partial melting and melt loss in felsic granulites in the Kutná Hora complex, Bohemian Massif (Czech Republic). Lithos, 125, 641–658.
- Nichols, G.T., and Wiebe, R.A. (1998) Desilication veins in the Cadillac Mountain granite (Maine, USA): a record of reversals in the SiO₂ solubility of H₂O-rich vapour released during subsolidus cooling. Journal of Metamorphic Geology, 16, 795–808.
- Nixon, P.H., Chapman, N.A., and Gurney, J.J. (1978) Pyrope-spinel (alkremite) xenoliths from kimberlite. Contributions to Mineralogy and Petrology, 65, 341–346.
- O'Brien, P.J. (2006) Type-locality granulites: high-pressure rocks formed at eclogite-facies conditions. Mineralogy and Petrology, 86, 161–175.

- (2008) Challenges in high-pressure granulite metamorphism in the era of pseudosections: reaction textures, compositional zoning and tectonic interpretation with examples from the Bohemian Massif. Journal of Metamorphic Geology, 26, 235–251.
- O'Brien, P.J., and Rötzler, J. (2003) High-pressure granulites: formation, recovery of peak conditions and implications for tectonics. Journal of Metamorphic Geology, 21, 3–20.
- O'Brien, P.J., Kröner, A., Jaeckel, P., Hegner, E., Żelanzniewicz, A., and Kryza, R. (1997) Petrological and isotopic studies on Palaeozoic high-pressure granulites, Góry Sowie Mts, Polish Sudetes. Journal of Petrology, 38, 433–456.
- Osanai, Y., Sajeev, K., Owada, M., Wilbert Kehelpannala, K.V., Bernard Prame, W.K., Nakano, N., and Jayatileke, S. (2006) Metamorphic evolution of high-pressure and ultrahigh-temperature granulites from the Highland Complex, Sri Lanka. Journal of Asian Earth Sciences, 28, 20–37.
- Ouzegane, K., Guiraud, M., and Kienast, J.R. (2003) Prograde and retrograde evolution in high-temperature corundum granulites (FMAS and KFMASH Systems) from In Ouzzal Terrane (NW Hoggar, Algeria). Journal of Petrology, 44 517–545
- Padovani, E.R., and Tracy, R.J. (1981) A pyrope-spinel (alkremite) xenolith from Moses Rock Dike: first known North American occurrence. American Mineralogist, 66, 741–745.
- Peper, J.D., and Pease, M.H. Jr. (1975) Geologic map of the Westford quadrangle, Connecticut. U.S. Geological Survey Quadrangle Map, GQ-1214.
- Perchuck, A.L. (2008) Unusual inclusions in garnet from the diamond-bearing gneiss of the Erzgebirge, Germany. Geochemistry International, 46, 296–303.
- Peterman, E.M., Snoeyenbos, D.R., Jercinovic, M.J., and Kylander-Clark, A. (2016) Dissolution-reprecipitation metasomatism and growth of zircon within phosphatic garnet in metapelites from western Massachusetts. American Mineralogist, 101, 1792–1806.
- Porter, B.S., Wiebe, R., Cheney, J.T. (1999) Regional and contact metamorphism of Paleozoic greenschist and pelites, Vinalhaven Island, Maine. Geological Society of America Abstracts with Programs, 31, A-61.
- Powell, R., and Sandiford, M. (1988) Sapphirine and spinel phase relationships in the system FeO–MgO–Al₂O₃–SiO₂–TiO₂–O₂ in the presence of quartz and hypersthene. Contributions to Mineralogy and Petrology, 98, 64–71.
- Putnis, A., and Austrheim, H. (2010) Fluid-induced processes: metasomatism and metamorphism. Geofluids, 10, 254–269.
- Putnis, A., and John, T. (2010) Replacement processes in the Earth's crust. Elements, 6, 159–164.
- Robinson, P. (1978) The Bronson Hill anticlinorium and Merrimack synclinorium in central Massachusetts—an Acadian "Pennine zone." Geological Society of America Abstracts with Programs, 10, 82.
- Robinson, P., and Tucker, R.D. (1982) The Merrimack Synclinorium in Northeastern Connecticut. American Journal of Science, 282, 1735–1744.
- Robinson, P., Tucker, R.D., Bradley, D., Berry, H.N. IV, and Osberg, P.H. (1998) Paleozoic orogens in New England, USA. GFF, vol. 120 (Pt. 2, June), p. 119–148. Stockholm.
- Rodgers, J. (1981) The Merrimack Synclinorium in Northeastern Connecticut. American Journal of Science, 281, 176–186.
- (1985) Bedrock Geological Map of Connecticut, scale 1:125,000. Connecticut Geological and Natural History Survey, Department of Environmental Protection, Hartford, Connecticut.
- Rogers, G.S. (1911) Geology of the Cortlandt Series and its emery deposits. New York Academy of Science Annals, 21, 11–86.
- Rötzler, J. (1992) The petrogenesis of pyroxene-free granulites and metapelites of the Saxonian granulite massif, Germany. Geotektonische Forschungen 77, 1–100 (in German)
- Rötzler, J., and Romer, R.L. (2001) P-T-t evolution of ultrahigh-temperature granulites from the Saxon Granulite Massif, Germany. Part I: Petrology. Journal of Petrology, 42, 1995–2013.
- Rudnick, R.L. (1995) Making continental crust. Nature, 378, 571-578.
- Ruiz-Cruz, M.D., and Sanz de Galdeano, C. (2013) Coesite and diamond inclusions, exsolution microstructures and chemical patterns in ultrahigh pressure garnet from Ceuta (Northern Rif, Spain). Lithos, 177, 184–206.
- Sack, R.O., and Ghiorso, M.S. (1991a) An internally consistent model for the thermodynamic properties of Fe–Mg-titanomagnetite-aluminate spinels. Contributions to Mineralogy and Petrology, 106, 474–505.
- ——— (1991b) Chromian spinels as petrogenetic indicators: Thermodynamics and petrological applications. American Mineralogist. 76, 827–847.
- Sakamaki, K., Sato, Y., and Ogasawara, Y. (2016) Hydrous Na-gamet from Garnet Ridge; products of mantle metasomatism underneath the Colorado Plateau. Progress in Earth and Planetary Science, 3, 20.
- Schreyer, W., Horrocks, P.C., and Abraham, K. (1984) High-magnesium staurolite in a sapphirine-garnet rock from the Limpopo Belt, Southern Africa. Contributions to Mineralogy and Petrology, 86, 200–207.
- Schumacher, J.C., Schumacher, R., and Robinson, P. (1989) Acadian metamorphism in central Massachusetts and south-western New Hampshire: evidence for contrasting P-T trajectories. In J.S. Daly, R.A. Cliff, and B.W.D. Yardley, Eds., Evolution of Metamorphic Belts, Geological Society Special Publication, 43, 453–460.
- Sengupta, P., Sen, J., Dasgupta, S., Raith, M., Bhui, U.K., and Ehl, J. (1999) Ultra-high

- temperature metamorphism of metapelitic granulites from Kondapalle, Eastern Ghats Belt: Implications for the Indo-Antarctic correlation. Journal of Petrology, 40, 1065–1087.
- Shaffer, M., Hacker, B.R., Ratschbacher, L., and Kylander-Clark, A.R.C. (2017) Foundering triggered by the collision of India and Asia captured in xenoliths. Tectonics. 36, 1913–1933.
- Shimpo, M., Tsunogae, T., and Santosh, M. (2006) First report of garnet-corundum rocks from southern India: Implications for prograde high-pressure (eclogite-facies?) metamorphism. Earth and Planetary Science Letters, 242, 111–129.
- Shulters, J.C., and Bohlen, S.R. (1989) The stability of hercynite and hercynite-gahnite spinels in corundum- or quartz-bearing assemblages. Journal of Petrology, 30, 1017–1031
- Smithies, R.H., and Champion, D.C. (1999) Late Archean felsic alkaline igneous rocks in the Eastern Goldfields, Yilgarn Craton, Western Australia: a result of lower crustal delamination? Journal of the Geological Society, London, 156, 561–576.
- Snoeyenbos, D.R., and Koziol, A.M. (2008) Exsolution phenomena of UHP type in Garnets From Western New England, USA. American Geophysical Union, Fall Meeting 2008, Abstract V31E-07.
- Snoeyenbos, D.R., Williams, M.L., and Hanmer, S. (1995) Archean high-pressure metamorphism in the western Canadian Shield. European Journal of Mineralogy, 7, 1251–1272.
- Sorger, D., Hauzenberger, C.A., Linner, M., Iglseder, C., and Finger, F. (2018) Carboniferous polymetamorphism recorded in paragneiss-migmatites from the Bavarian Unit (Moldanubian Superunit, Upper Austria): implications for the tectonothermal evolution at the end of the Variscan orogeny. Journal of Petrology, egy063.
- Štípská, P., and Powell, R. (2005) Does ternary feldspar constrain the metamorphic conditions of high-grade meta-igneous rocks? Evidence from orthopyroxene granulites, Bohemian Massif. Journal of Metamorphic Geology, 23, 627–647.
- Tchameni, R., Mezger, K., Nsifa, N.E., and Pouclet, A. (2001) Crustal origin of Early Proterozoic syenites in the Congo Craton (Ntem Complex), South Cameroon. Lithos, 57, 23–42.
- Thomson, J.A. (2001) A counterclockwise P-T path for anatectic pelites, south-central Massachusetts. Contributions to Mineralogy and Petrology, 141, 623–641.
- Tracy, R.J., Robinson, P., and Thompson, A.B. (1976) Garnet composition and zoning in the determination of temperature and pressure of metamorphism, central Massachusetts. American Mineralogist, 61, 762–775.
- van Roermund, H.L.M., Drury, M.R., Barnhoorn, A., and De Ronde, A. (2000) Non-silicate inclusions in garnet from an ultra-deep orogenic peridotite. Geological Journal, 35, 209–229.
- Weller, O.M., and St-Onge, M.R. (2017) Record of modern-style plate tectonics in the Palaeoproterozoic Trans-Hudson orogen. Nature Geoscience, 10, 305–311.
- Wheller, C.J., and Powell, R. (2014) A new thermodynamic model for sapphirine: calculated phase equilibria in K₂O–FeO–MgO–Al₂O₃–SiO₂–H₂O–TiO₂–Fe₂O₃. Journal of Metamorphic Geology, 32, 287–299.
- White, R.W., Powell, R., and Clarke, G.L. (2002) The interpretation of reaction textures in Fe-rich metapelitic granulites of the Musgrave Block, central Australia: constraints from mineral equilibria calculations in the system K₂O–FeO–MgO–Al₂O₃–SiO₂–H₂O–TiO₂–Fe₂O₃. Journal of Metamorphic Geology, 20, 41–55.

- White, R.W., Powell, R., Holland, T.J.B., Johnson, T.E., and Green, E.C.R. (2014a) New mineral activity-composition relations for thermodynamic calculations in metapelitic systems. Journal of Metamorphic Geology, 32, 261–286.
- White, R.W., Powell, R., and Johnson, T.E. (2014b) The effect of Mn on mineral stability in metapelites revisited: new a-x relations for manganese-bearing minerals. Journal of Metamorphic Geology, 32, 809–828.
- Willner, A.P., Rötzler, K., and Maresch, W.V. (1997) Pressure-temperature and fluid evolution of quartzo-feldspathic metamorphic rocks with a relic high-pressure, granulite-facies history from the Central Erzgebirge (Saxony, Germany). Journal of Petrology, 38, 307–336.
- Wintsch, R.P., Sutter, J.F., Kunk, M.J., Aleinikoff, J.N., and Dorais, M.J. (1992) Contrasting P-T-t paths: Thermochronologic evidence for a Late Paleozoic final assembly of the Avalon Composite Terrane in the New England Appalachians. Tectonics, 11, 672–689.
- Wintsch, R.P., Aleinikoff, J.N., and Walsh, G.J. (2009) Late Silurian deposition and Late Devonian metamorphism of Gander Cover at the Southern end of the Central Maine Terrane: Evidence from SHRIMP analysis of detrital zircons. Geological Society of America Abstracts with Programs, 41, 98.
- Wu, C., and Chen, H. (2015) Revised Ti-in-biotite geothermometer for ilmenite- or rutile-bearing crustal metapelites. Science Bulletin, 60, 116–121.
- Yao, Y., Ye, K., Liu, J., Cong, B., and Wang, Q. (2000) A transitional eclogite- to high pressure granulite-facies overprint on coesite-eclogite at Taohang in the Sulu ultrahigh-pressure terrane, Eastern China. Lithos, 52, 109–120.
- Ye, K., Cong, B., and Ye, D. (2000) The possible subduction of continental material to depths greater than 200 km. Nature, 407, 734–736.
- Zegers, T.E., and van Keken, P.E. (2001) Middle Archean continent formation by crustal delamination. Geology, 29, 1083–1086.
- Zhang, R.Y., Zhai, S.M., Fei, Y.W., and Liou, J.G. (2003) Titanium solubility in coexisting garnet and clinopyroxene at very high pressure: the significance of exsolved rutile in garnet. Earth and Planetary Science Letters, 216, 591–601.
- Zhao, G., Cawood, P.A., Wilde, S.A., and Lu, L. (2001) High-pressure granulites (retrograded eclogites) from the Hengshan Complex, North China Craton: Petrology and tectonic implications. Journal of Petrology, 42, 1141–1170.
- Zulauf, G., Dörr, W., Fiala, J., Kotková, J., Maluski, H., and Valverde-Vaquero, P. (2002) Evidence for high-temperature diffusional creep preserved by rapid cooling of lower crust (North Bohemian shear zone, Czech Republic). Terra Nova, 14, 343–354.

MANUSCRIPT RECEIVED MARCH 8, 2018
MANUSCRIPT ACCEPTED JULY 16, 2018
MANUSCRIPT HANDLED BY THOMAS MUELLER

Endnote:

¹Deposit item AM-18-116543, Supplemental Tables. Deposit items are free to all readers and found on the MSA web site, via the specific issue's Table of Contents (go to http://www.minsocam.org/MSA/AmMin/TOC/2018/Nov2018_data/Nov2018_data.html).